Int. J. Multiphase Flow Vol. 8, No. 2, pp. 93–124, 1982
Printed in Great Britain.

0301-9322/82/020093-32$03.00/0
Pergamon/Elsevier

ON THE DEVELOPMENT OF AN OBJECTIVE FLOW REGIME INDICATOR

M. A. VINCE and R. T. LAHEY, JR.

Department of Nuclear Engineering, Rensselaer Polytechnic Institute, Troy, NY 12181, U.S.A.

(*Received* 3 *October* 1980; *in revised form* 19 *June* 1981)

Abstract—A high intensity dual beam X-ray system was designed and constructed to make chordal-average void fraction measurements. This X-ray system employed a DC excited tube filament, full wave rectification and high voltage filtering to produce a stable photon source. The large photon flux produced by the X-ray system allowed analog linearization of the signal.

A series of chordal-average void fraction measurements were made and used to generate probability density functions (PDF) and power spectral density (PSD) functions. The first four moments associated with these distributions were studied as possible flow regime indicators.

The moments of the PDF indicated the various flow regime transitions. The moments of the PSD also show some flow regime transition information, but were sensitive to liquid phase velocity. The PDF variance, or second moment about the mean, was found to be the best indicator of flow regime. A variance of 0.04 appear to adequately discriminate between the bubbly, slug and annular flow regimes for low pressure air/water flow in a 2.54 cm I.D. vertical tube.

1. INTRODUCTION

1.1 *Background*

Vertical two-phase flow is normally classified into four basic flow regimes: (1) bubbly; (2) slug; (3) churn-turbulent; (4) annular. These flow regimes are shown schematically in figure 1.

Bubbly flow is characterized by small, discrete bubbles surrounded by liquid. This flow regime usually occurs at low void fraction.

Slug flow consists of slugs of liquid and bubbles separated by regions of high vapor content. The vapor phase normally appears as large, spherical-capped bubbles, followed by a collection of much smaller voids, in bubbly form. At the lower flow rates, this flow regime represents an intermediate stage between bubbly and annular flow.

Churn-turbulent flow is a special case which normally occurs at high flow rates, and is characterized by chaotic motion between the phases. This flow regime can be considered to be an intermediate stage between the bubbly and annular flow regimes at high flow rates. Liquid bridging, a characteristic of slug flows, is still observed, however it is quite intermittent.

Annular flow occurs at high void fractions and is characterized by a central vapor core surrounded by an annulus of liquid. Liquid phase entrainment (i.e. droplets moving in the vapor core) is also frequently observed. Roll waves may move along the interface, however the liquid bridging, observed in slug flow, does not exist.

Flow regime maps represent a convenient way to indicate the phase distribution of a two-phase mixture. Flow regime boundaries can be indicated on a plot of parameters commonly measured or calculated.

One of the first vertical flow regime maps was proposed by Govier *et al.* (1957, 1958). They investigated the effects of pipe diameter and air/water flow rates on flow pattern, void fraction and pressure drop. It was found that a change in pressure drop accompanies a change of flow regime. Thus Govier *et al.* (1957, 1958) correlated the superficial water velocity and the air-to-water volumetric flux ratio. Their results are based on the premise tht the flow regime transitions occur at inflection points of the void fraction curves and at minimums in the pressure drop curves.

Griffith & Wallis (1961) proposed a flow regime map for vertical fully-developed slug flow. A plot of the relative gas flow rate vs the mixture Froude number results in a curve separating annular and bubbly flow from fully developed slug flow.

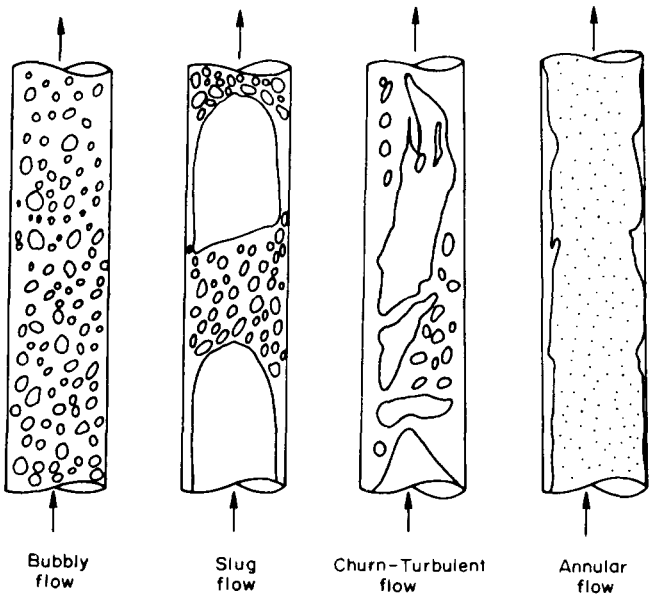

Figure 1. The four flow regimes observed in vertical two-phase flow.

Hubbard & Dukler (1966) measured the pressure fluctuations at the wall of a horizontal pipe, containing various two-phase mixtures. The time response of the pressure transducer was digitized and the power spectral density (PSD) function was computed from the autocorrelation. The resulting power spectrum was then classified into three broad categories. The various flow regimes were categorized by considering their energy distribution. It appears that this work represented the first attempt at objective classification of flow regimes, although related work has been performed by Nishikawa *et al.* (1969) and Kutateladze *et al.* (1972).

Taitel *et al.* (1980) developed pseudo-analytical models for predicting flow regime transitions in vertical flow. These models are based on the physical mechanisms associated with each transition. The effects of fluid properties and pipe size were also considered. It should be noted that the Taitel–Dukler flow regime map assumes that the bubbly-slug flow regime transition occurs at constant global void fraction while the slug-annular flow regime transition takes place at a constant superficial vapor velocity, independent of the superficial liquid velocity and pipe diameter.

The first photon attenuation technique used for flow regime identification was apparently developed by Jones & Zuber (1975). This system utilized a dual beam X-ray device. Air and water, flowing vertically in a two-dimensional test section, were used to achieve the two-phase conditions. The probability density function (PDF) and the power spectral density (PSD) function were formed from the digitized data set collected. Jones & Zuber observed that bubbly flow was characterized by a single, low void, peak in the PDF. Slug flow had a bimodal PDF; the low void mode corresponding to the vapor in the liquid slug and the high void peak corresponding to the spherical-capped Taylor bubbles. Annular flow displayed a single peak, similar to bubbly flow, but at high void fraction. Jones & Zuber did not attempt to deduce an objective flow regime transtion from his data.

1.2 *Flow regime characterization*

The statistical content of a stochastic process frequently yields valuable information about the nature of the process. Indeed, Pattern Recognition Theory (Caulfield *et al.* 1980 and Young & Calvert 1974) is based on using various measures of the statistical process to infer information of interest. In particular, it is known that the moments of the various density function histograms completely quantify the information in the histograms.

Four moments are commonly associated with any distribution: (1) The mean, or first moment about the origin. (2) The variance, or second moment about the mean. (3) The skewness, or third moment about the mean. (4) The kurtosis, or fourth moment about the mean. The mean is the average value of a distribution. Variance is a measure of the distribution about the mean.

The third moment, skewness, is a measure of the asymmetry of a distribution. A symmetric distribution, such as a normal distribution, has zero skewness since the mean and the median coincide. A unimodal distribution, which has a median to the left of the mean, (i.e. it is skewed to the left) has a negative skewness. If the distribution is skewed to the right, it will have a positive skewness. This moment is usually normalized by the variance to the 1.5 power. The resulting value is called the coefficient of skewness, and relates the skewness to the spread of the distribution.

Kurtosis, the fourth moment, is a measure of the distribution's peakedness. Similar to the skewness, this moment is often normalized by the square of the variance. The resultant parameter is called the coefficient of kurtosis. The normal distribution is mesokurtic (i.e. it has a coefficient of kurtosis equal to three). A distribution with a coefficient of kurtosis less than three is called platykurtic. These distributions are flatter than a normal distribution. Distributions with more peakedness than a normal distribution are called leptokurtic, and have a coefficient of kurtosis greater than three.

These moments have physical significance and can be related to the various two-phase flow regimes. The variance of the void distribution should be small in bubbly and annular flows. These flows should also be leptokurtic and possess large (positive or negative) skewness. Slug flow void distributions, on the contrary, should have a large variance but small skewness. The slug flow void distribution is normally platykurtic. Flow regime identification should thus be possible with these moments.

Calculation of the moments of a discrete distribution is straight-forward. The mean is the sum of the products of the possible void fractions α_i and their associated probabilities p_i

$$\alpha = \sum_{i=1}^{N} \alpha_i p_i. \qquad [1]$$

Higher moments about the mean M_n are calculated in similar fashion,

$$M_n = \sum_{i=1}^{N} (\alpha_i - \alpha)^n p_i. \qquad [2]$$

The coefficients of skewness C_{M_3} and kurtosis C_{M_4} are formed by dividing the skewness M_3 and kurtosis M_4 by the variance M_2 raised to the appropriate power. That is,

$$C_{M_3} = \frac{M_3}{M_2^{1.5}} \qquad [3]$$

$$C_{M_4} = \frac{M_4}{M_2^2}. \qquad [4]$$

Later reference to skewness and kurtosis should be taken to mean the coefficient of skewness or the coefficient of kurtosis.

These moments can be calculated from the measured chordal void fraction, and can be used to infer information on flow regime. The next section will be concerned with the technique actually used at RPI to measure the instantaneous chordal-average void fraction.

2. DESIGN OF THE EXPERIMENT AND INSTRUMENTATION

2.1 *Technique*

Many techniques are available for void fraction measurement (Hsu 1977, Lahey 1978). X-ray attenuation was selected in this study to provide the statistical data required for the calculation of the PDF and PSD. The technique developed provided the fast response and accuracy necessary.

Several design criteria were incorporated into the X-ray system developed at RPI for chordal-average void measurement.

(1) Relative chordal-average (along the test section diameter) void fraction error, $\Delta\alpha/\alpha$, of less than five percent in one millisecond, for the lowest void fraction of interest.
(2) Test and reference beams from the same photon source, to reduce common mode noise.
(3) Analog linearization of the void signal before digitization, to eliminate dynamic bias.
(4) DC excitation of the X-ray tube's filament for photon output stability.
(5) Mobility so that a conduit could be scanned laterally and vertically.

A system based on the above criteria can accurately measure the instantaneous chordal-average void fraction and provide data for the formation of the PDF and PSD.

2.2 *Dual Beam X-Ray System*

Monoenergetic radiation attenuation follows the well known relationship known as Beer's Law.

$$I = I_0 \exp(-\bar{\mu}x) \tag{5}$$

where I_0 is the photon intensity incident on the test section (photon/cm^2 s) and $I(x)$ is the intensity at distance x into the media (photons/cm^{2}s). The two-phase attenuation coefficient ($\bar{\mu}$) can be expressed as,

$$\bar{\mu}x = \mu_G x_G + \mu_L x_L \tag{6}$$

where μ_G is the vapor attenuation coefficient (cm^{-1}) and μ_L is the liquid attenuation coefficient. This expression can be substituted into [5] to yield,

$$I = I_0 \exp -(\mu_G x_G + \mu_L x_L). \tag{7}$$

The attenuation coefficient of the vapor, μ_G, is usually much less than the attenuation coefficient for the liquid phase. Thus, for the (atmospheric) conditions of the experiment reported herein, [7] reduces to,

$$I = I_0 \exp(-\mu_L x_L) \tag{8}$$

Dual beam systems (Smith 1971, Jones & Zuber 1975) use a reference beam to compensate for variations in X-ray tube photon output. This type of set-up uses two beams from the same source: one passing through the two-phase mixture, and the other passing through a reference attenuator.

Previous work (Lahey *et al.* 1978) has shown that the instantaneous chordal-average void fraction α is given by a linearized expression of the form,

$$\alpha(t) = \frac{R(t) - R_L}{R_G - R_L} \tag{9a}$$

where

$$R(t) \overset{\Delta}{=} \ln\{V_s^*/V_r^*\} \tag{9b}$$

The X-ray system employed in this experiment is shown schematically in figure 2. It features full-wave rectification and high voltage filtering to insure a stable high voltage supply. Moreover, the X-ray tube filament is excited by a battery current source to insure photon emission stability.

Analog signal processing for this system, which follows the analysis of Lahey *et al.* (1978), is shown schematically in figure 3. The current output from the test and reference photomultipliers were fed, via shielded cables, to an analog devices model 756-P logarithmic ratio module. This solid state device was temperature compensated and can cover a dynamic range of 7 decades with an error less than ±1%. A DC bias voltage was applied to the reference signal to improve the signal-to-noise ratio (Lahey *et al.* 1978).

Chordal-average X-ray measurements were made in low (i.e. atmospheric) pressure air/water flow. A 2.54 cm dia. vertical plexiglass tube contained the two-phase mixture and allowed for direct observation. A more detailed description of the test loop and X-ray system has been given by Vince & Lahey (1980).

2.3 *Error analysis*

Two types of errors are normally associated with void fraction measurements; static and dynamic. Static error is due to the geometry and count statistics associated with the measurement. Dynamic error may be caused by improper averaging of the phenomena under study.

2.3.1 *Static error.* The static error may be calculated from geometric and counting statistics associated with the X-ray system. Malaviya & Lahey (1980) have developed an expression for the static error associated with a dual beam X-ray system.

$$\left(\frac{\Delta\alpha}{\alpha}\right)^2 = \frac{4\left(\frac{R_{SD}}{R_{ST}}\right)^2 (1-\alpha+\alpha^2)\exp[2\mu_w T + \mu_L C + \alpha(\mu_G - \mu_L)C]}{A_d \theta \epsilon I_0 \mu_L C^2 \alpha^2} \qquad [10]$$

where A_d is the area of the detector which is intersected by the photon beam, R_{SD} is the distance from source to detector (cm) R_{SL} is the distance from the source to the test section (cm) θ is the integration time μ_w is the attenuation coefficient of the test section walls (cm^{-1}) C is the chord length through the two phase mixture and T is the wall thickness of the conduit. This expression can be evaluated at each chordal position to yield the relative chordal-average void fraction error at that location. In this work the following parameters were utilized in the evaluation of the static error: $\theta = 1$ ms, $\epsilon = 0.70$ and $I_0 = 4.5 \times 10^9$ photons/cm^s-s.

Figure 4 shows the relative error as a function of chordal void fraction, associated with each chordal position, indicated in figure 5. The curves shown in figure 4 account for the variation in conduit wall thickness and pathlength at the various chordal positions for the 2.54 cm dia. plexiglass test section used in the RPI study. The centerline chord produces the most accurate results since the largest portion of the X-ray beam is attenuated in the two-phase mixture. In contrast, the wall chord contains the largest relative error.

The absolute error can be calculated by multiplying the relative error by the associated chordal-average void fraction. These results are illustrated in figure 6 for a sample time (θ) of 1 ms. It can be seen that the design and operating conditions of this X-ray system produce measurements with acceptably small static error.

2.3.2 *Dynamic error.* Dynamic error results because the logarithm of the time-average value of the measurement is not equal to the time-average of the logarithm of the measurement. Most photon densitometers operate in the pulse mode; that is, they count single events. The relatively small source strength associated with gamma ray devices make this type of signal processing necessary.

X-ray systems yield very high equivalent source strength. So high in fact that one can work

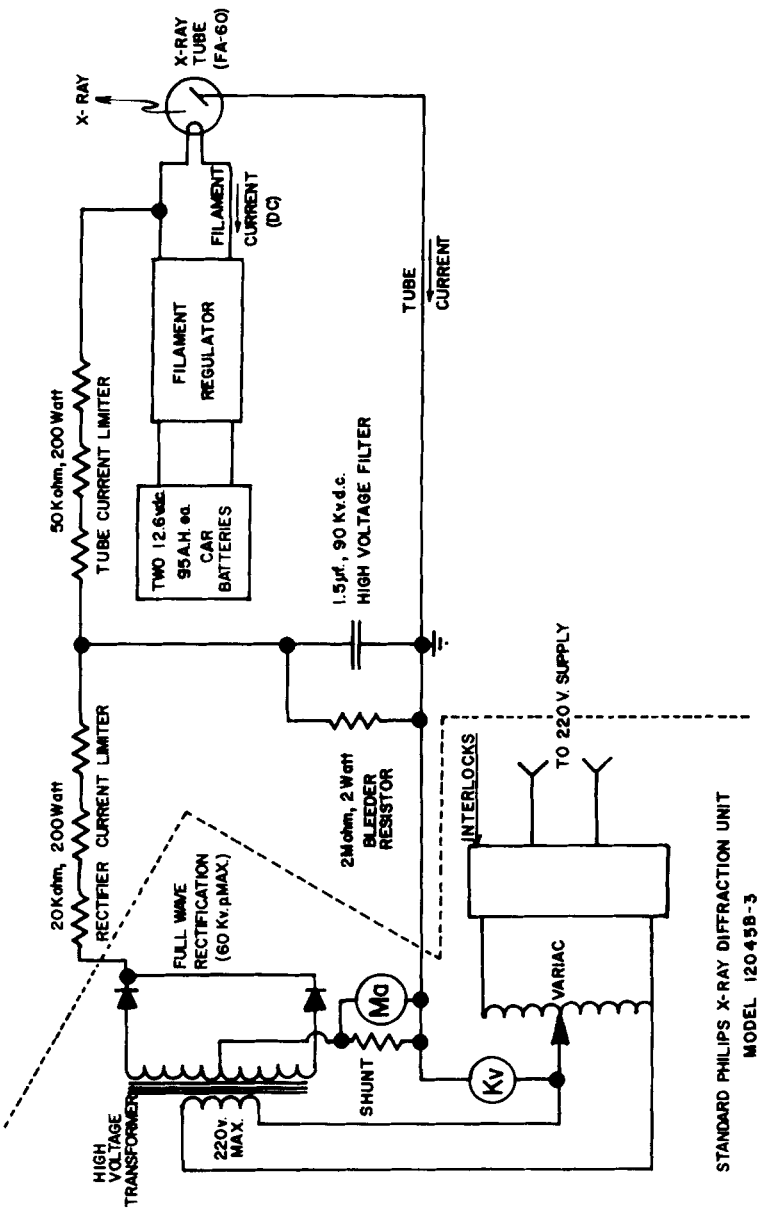

Figure 2. A schematic of the Philips X-ray diffraction unit as modified for chordal void fraction measurements.

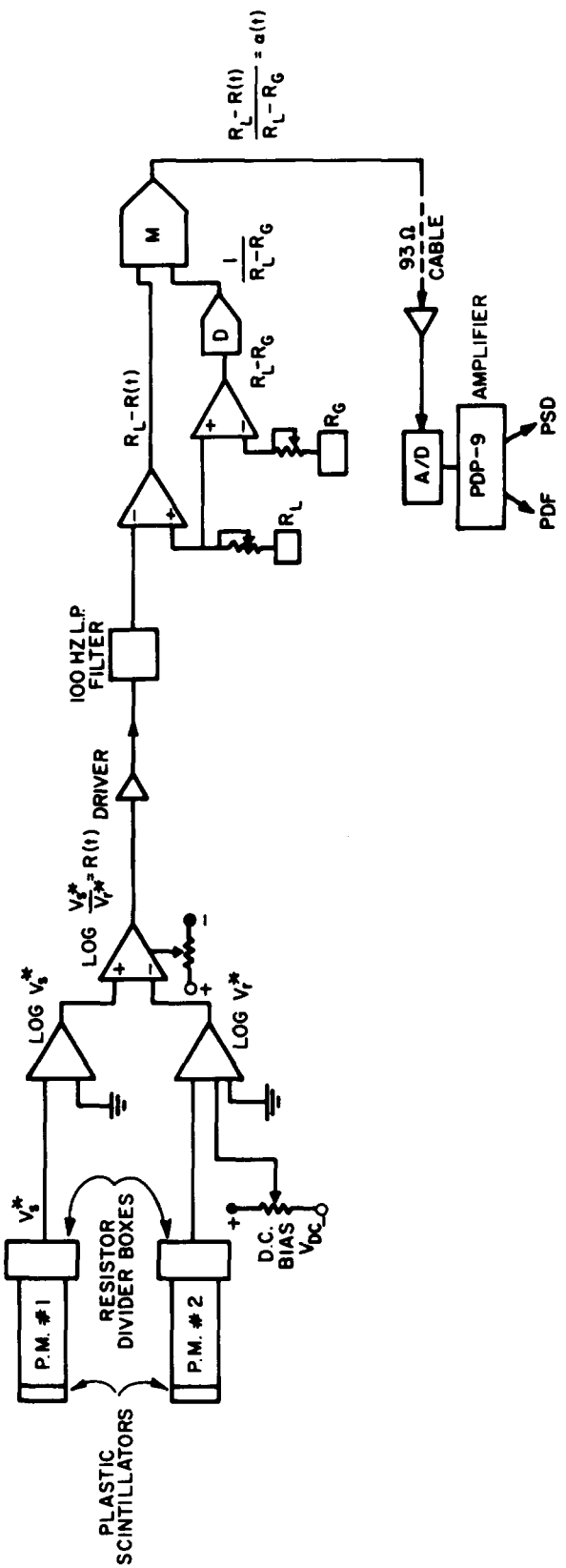

Figure 3. A schematic of the analog signal processing associated with the dual beam X-ray system.

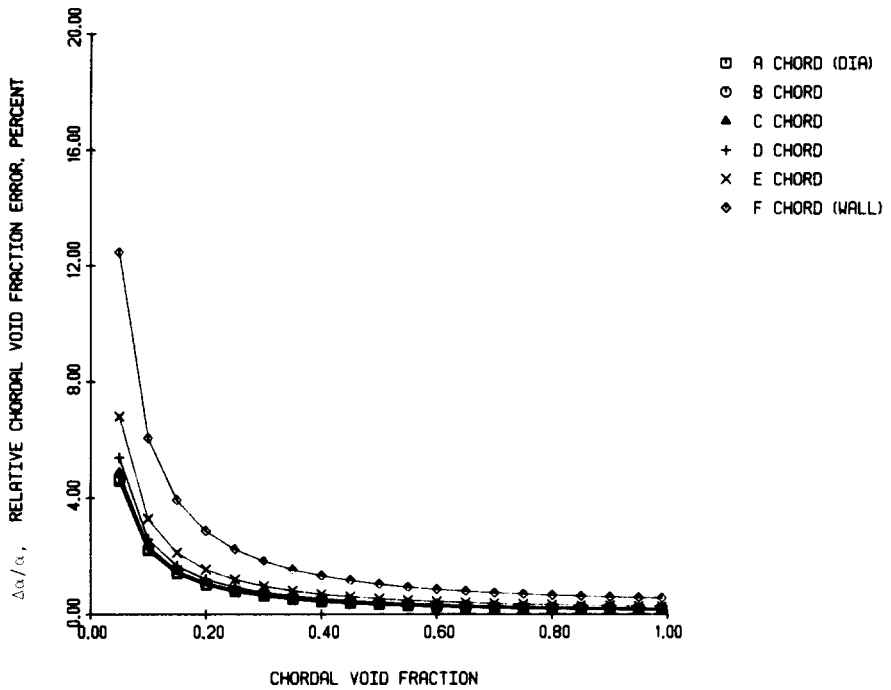

Figure 4. The relative chordal void fraction error ($\Delta\alpha/\alpha$) vs chordal void fraction.

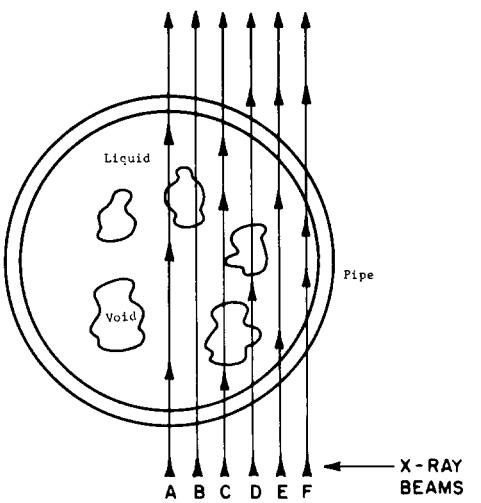

Figure 5. The six chords at which chordal void fraction measurements were made.

in the current mode, and thus the logarithms of the analog signal can be taken electronically† before data processing. Hence the measurement signal is linearized prior to time-averaging. Due to this linearization, dynamic error was not present in the X-ray measurements.

3. PDF AND PSD RESULTS

Comprehensive air/water two-phase flow chordal-average void fraction data were taken using the X-ray system. This data included zero and non-zero liquid flow cases. In all, forty-nine sets of data were acquired and processed. Each set consisted of six chordal measurements,

†The Analog Devices Model 756–P logarithmic ratio module utilized has a minimum frequency response of 0–1 kHz, making it more than adequate to resolve the phenomena of interest in this study.

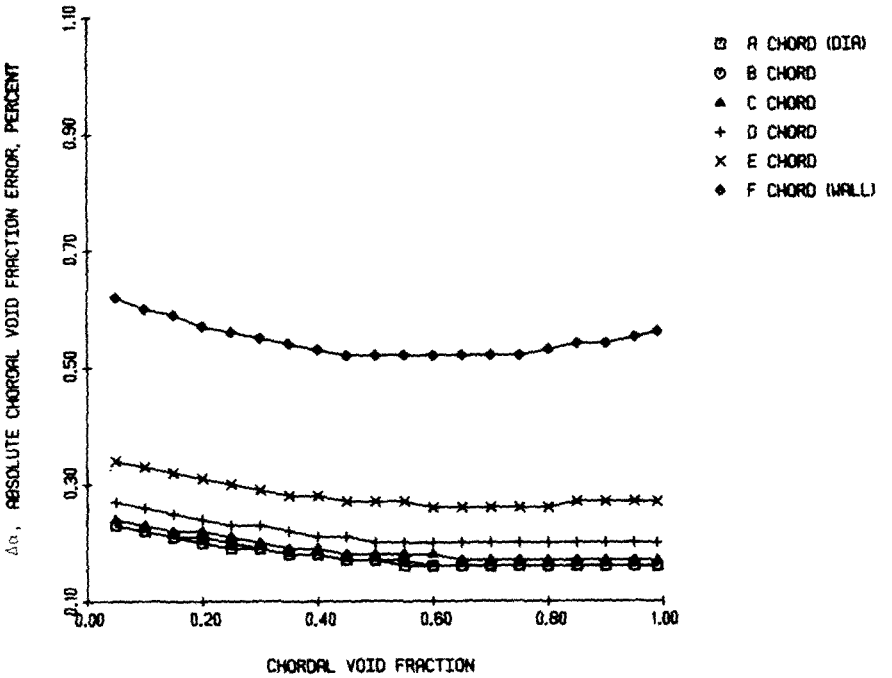

Figure 6. The absolute chordal void fraction error, $\Delta\alpha$ vs chordal void fraction.

including one along the diameter and one adjacent to the tube wall. The flow was found to be axisymmetric; thus data was only taken on one side of the tube. A plot of the air/water superficial velocities measured are shown in figure 7. The flow regimes shown here were determined visually. It can be noted that the data is concentrated in the regions in which flow regime transition takes place. For ease of display, all data taken at zero liquid superficial velocity has been placed at one-thousandth of a meter per second.

Each measurement consisted of 12,800 instantaneous void fraction readings at each chordal location. These data were collected at a rate of two hundred samples per second. A sixty-four

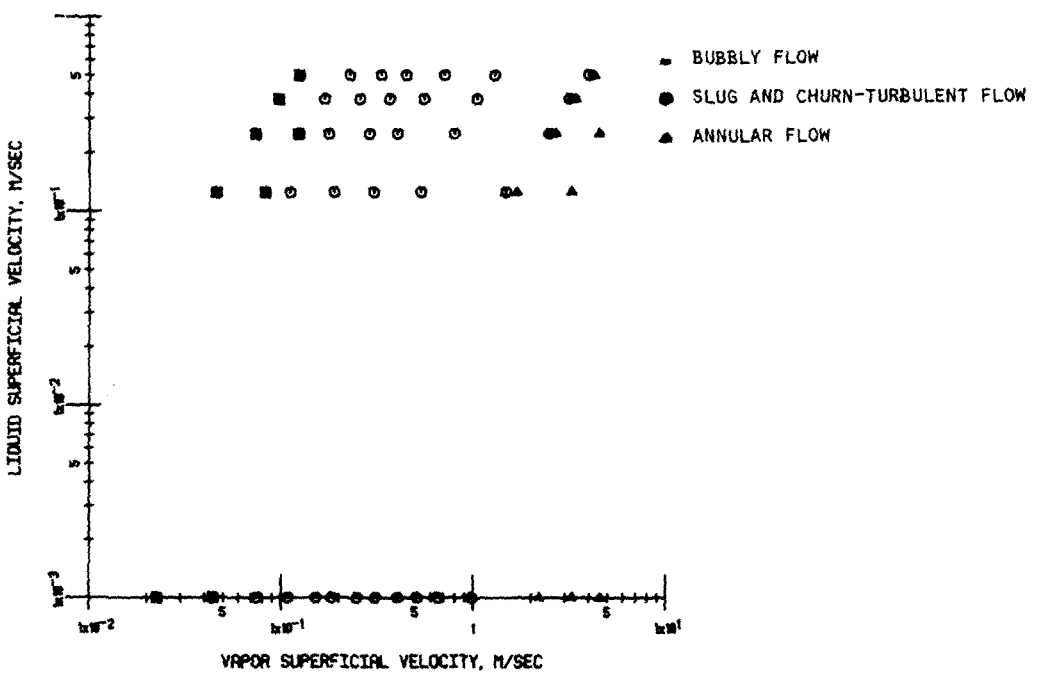

Figure 7. A flow regime map based on visual observation of the two-phase flow.

second sample time was determined to be large enough to insure a statistically stationary chordal-average void fraction for all flow regimes tested.

The normalized PDF were formed from all the data points acquired in each chordal void measurement. This histogram was further analyzed by computing the various moments associated with it.

The first 1024 points were used in forming the PSD because of the limitations on the data processing computer's central memory. A sampling frequency of two hundred per second results in a Nyquist frequency of one hundred hertz (i.e. one-half the sampling rate). To minimize aliasing errors, the break frequency of the four pole active low pass filter was set at 100 hz. This data set size, and the associated Nyquist frequency, set the frequency resolution at slightly greater than one-half hertz. The moments of the PSD were calculated in a fashion identical to the PDF. Different parts of the full data set were ensemble averaged to insure that the first 1024 point set produced a representative power spectrum.

The PSDs were normalized using the method suggested by Bendat & Piersol (1971),

$$\mathrm{PSD}(f) \triangleq \frac{2}{T_r}\left|(\mathrm{Re}(f))^2 + (\mathrm{Im}(f))^2\right| \qquad [11]$$

where, T_r is the record length of data, f is the frequency (H_3), Re(f) is the real part of the PSD and Im(f) is the imaginary part of the PSD as a function of the frequency.

The factor of 2 is applied because the data is strictly real. This normalization yields what is referred to on the following figures as the "normalized amplitude".

The effects of Hamming and Hanning windows (Blackman & Tukey 1958) were also investigated. Application of a data window changed the total amplitude of the spectrum, but did not change its shape. Thus, no windowing was performed on the data presented herein.

The PDF shown in figure 8 was measured for zero void fraction (i.e. liquid-only conditions). The PDF appears as a sharp spike at zero void. As in previous experiments of this type (Jones & Zuber 1975), this distribution is a normal distribution. Since the X-ray system developed at RPI had a very stable photon output, the observed standard deviation for all liquid conditions

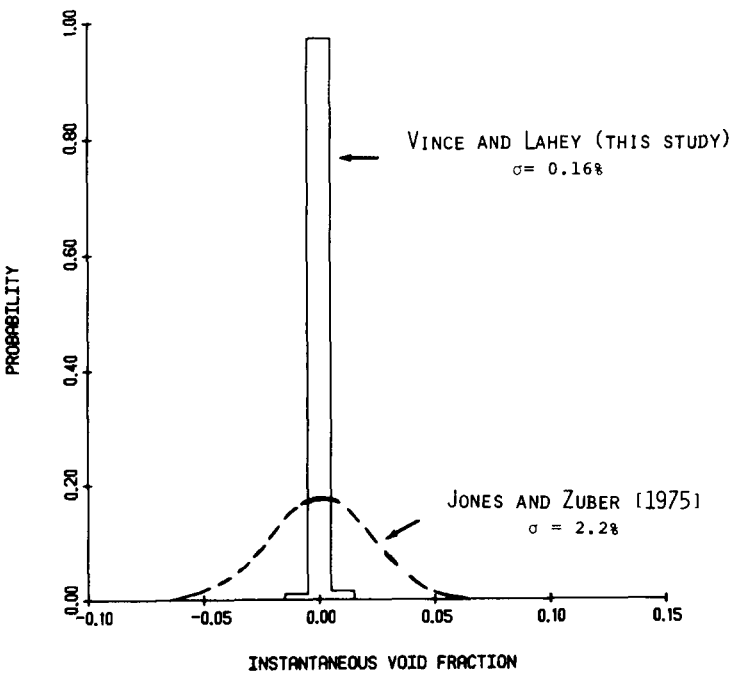

Figure 8. The PDF for single phase liquid flow i.e. void fraction equal zero.

was only 0.16 percent. This is considerably less than the 2.2 percent measured by Jones & Zuber (1975) at zero void fraction.

3.1 *Visual data*

Photographs and visual observation were taken of each two-phase condition studied. At low liquid velocity, visual flow regime identification is easily made for bubbly or slug flow. Higher liquid velocity makes visual flow regime distinction more difficult.

Churn-turbulent flow is relatively easy to observe, however, the transition from slug to churn-turbulent flow is very difficult to detect visually.

The conclusions drawn from visual observation can differ, depending on the observer. Indeed, visual methods are quite subjective and accurate conclusions regarding flow regime boundaries cannot normally be made.

3.1.1 *Centerline PDF and PSD distributions.* Photographs of some of the two-phase mixtures studied are displayed with the diametric PDF and PSD. The diameter distributions were selected because they are representative of the conditions prevailing in the entire pipe.

The PDF, PSD and two-phase mixture associated with an area-averaged void fraction of 13 percent and a liquid superficial velocity of 0.12 m/sec is illustrated in figure 9. A unimodal PDF, typical of bubbly flow, is observed. A sharp peak is also observed at zero void fraction due to the measurement associated with the liquid phase only. Jones & Zuber (1975) did not observe this peak, apparently because of their collimations and because fluctuations in their X-ray intensity limited resoluton.

The PSD shown in figure 9 is broadband and of low amplitude. Other liquid flow cases are very similar except that the bandwidth increases with liquid velocity. This is expected since bubbles move at a higher velocity as j_L is increased.

For 26 percent area-averaged void fraction, the PDF, PSD and two-phase pictures are shown in figures 10–14 for liquid superficial velocities of 0.0, 0.12, 0.25, 0.37, and 0.5 m/sec, respectively. The PDF associated with zero liquid flow is very broad due to the presence of Taylor bubbles. As found at lower void fraction, the onset of liquid flow reduces the breadth of the PDF; this is shown in figure 11. The increasing air flow associated with an increasing liquid flow, to maintain a constant area-average void fraction, promotes the transition to slug flow. A very broad PDF is observed for a superficial velocity of 0.25 m/sec as shown in figure 12. Ultimately, the increased liquid flow cannot suppress the transition to slug flow and the PDF becomes bimodal. These results are clearly shown in figures 13 and 14.

The PSDs associated with this void fraction show an interesting trend. All PSDs for this void fraction show characteristic peaks. As expected, the position of these peaks increase in frequency with increasing liquid velocity. Some of the peaks are rather broad; especially those shown in figures 13 and 14.

Jones & Zuber (1975) has previously attempted to discriminate between flow regimes by looking at the number of modes in the PDF. The PDFs and photographs shown in figures 10–14 indicate that the transition from bubbly to slug flow in a circular conduit can be very gradual. Thus discrimination based on the number of modes will be quite subjective. Jones & Zuber used a 2-dimensional conduit geometry which simplified data interpretation. The circular conduit geometry used in this study indicates that the number of modes possessed by a PDF is not adequate for flow regime identification. However, as will be discussed later, calculations of the moments can provide an objective indicator.

Fully-developed slug flow is obvious in figure 15 for 41 percent area-averaged void fraction, and a zero liquid superficial velocity. The PDF is bimodal, as expected, regardless of liquid velocity.

The PSD also shows behavior characteristic of slug flow. That is, a sharp peak of large magnitude is observed at low frequency. As expected, other data (not shown here) shows that the PSD peak's location moves to higher frequency as the liquid velocity is increased.

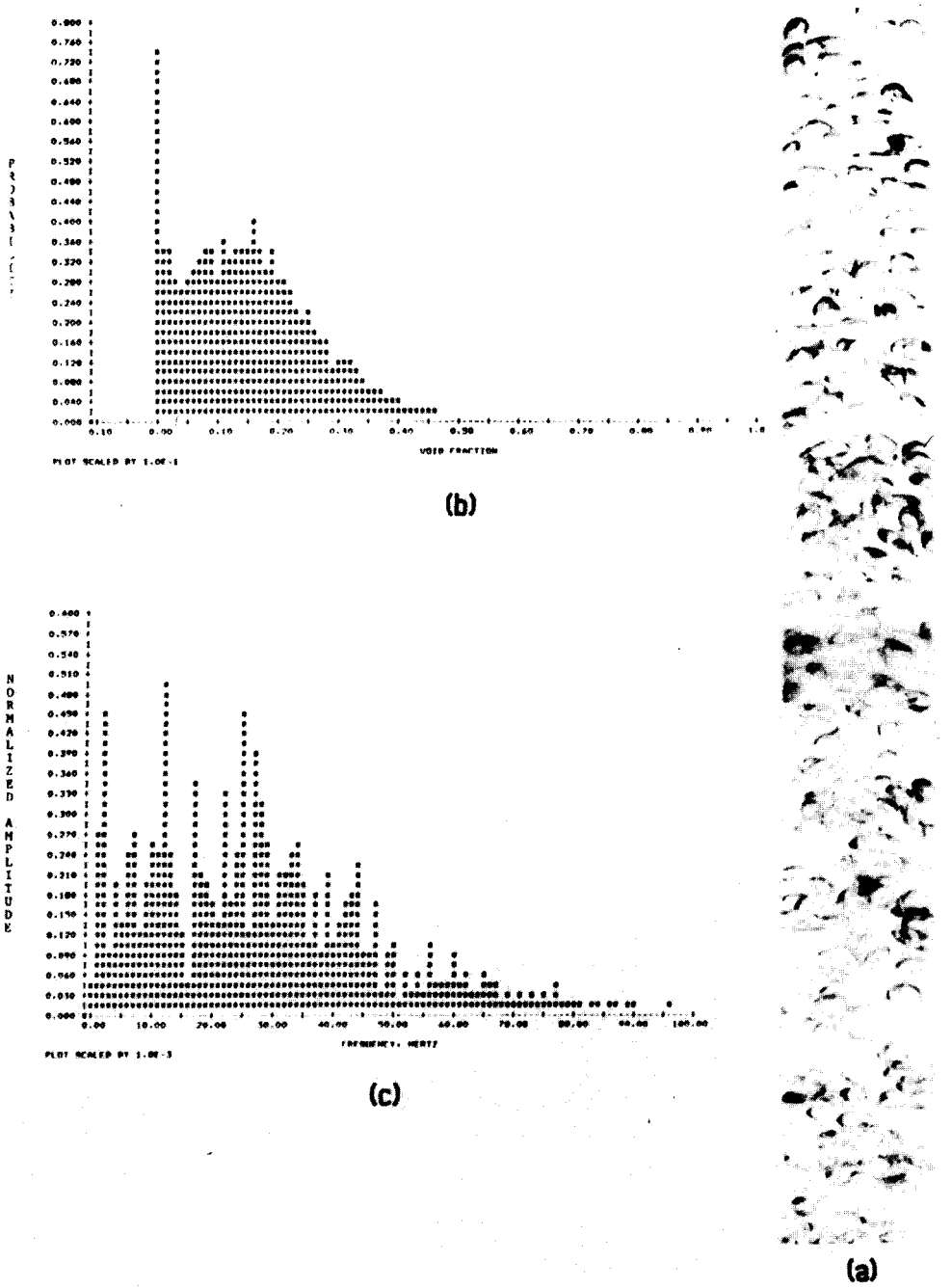

Figure 9. A photograph (a), diameter PDF (b), and diameter PSD (c), for 13 percent area-averaged void fraction, $j_L = 0.12$ m/sec, $j_G = 0.045$ m/sec.

Figures 16–20 illustrate the PDF, PSD and photographs for 68 area-averaged void fraction. The liquid superficial velocities shown were 0.0, 0.12, 0.25, 0.37, and 0.5 m/sec, respectively. The zero liquid flow case has a bimodal PDF and a single low frequency peak in the PSD. Liquid flow increases cause unimodal PDF typical of annular flow. Note that the PSD is broadened and reduced in amplitude, as would be expected in annular flow.

3.1.2 *Moments of the probability density function (PDF) data.*

3.1.2.1 *Zero liquid flow data.* A plot of the PDF variance as a functon of chordal-average void fraction is indicated in figure 21. The curve is relatively smooth in the low void region where the bubbly-slug transition is expected, (at 20–30 percent chordal-average void fraction). However, a

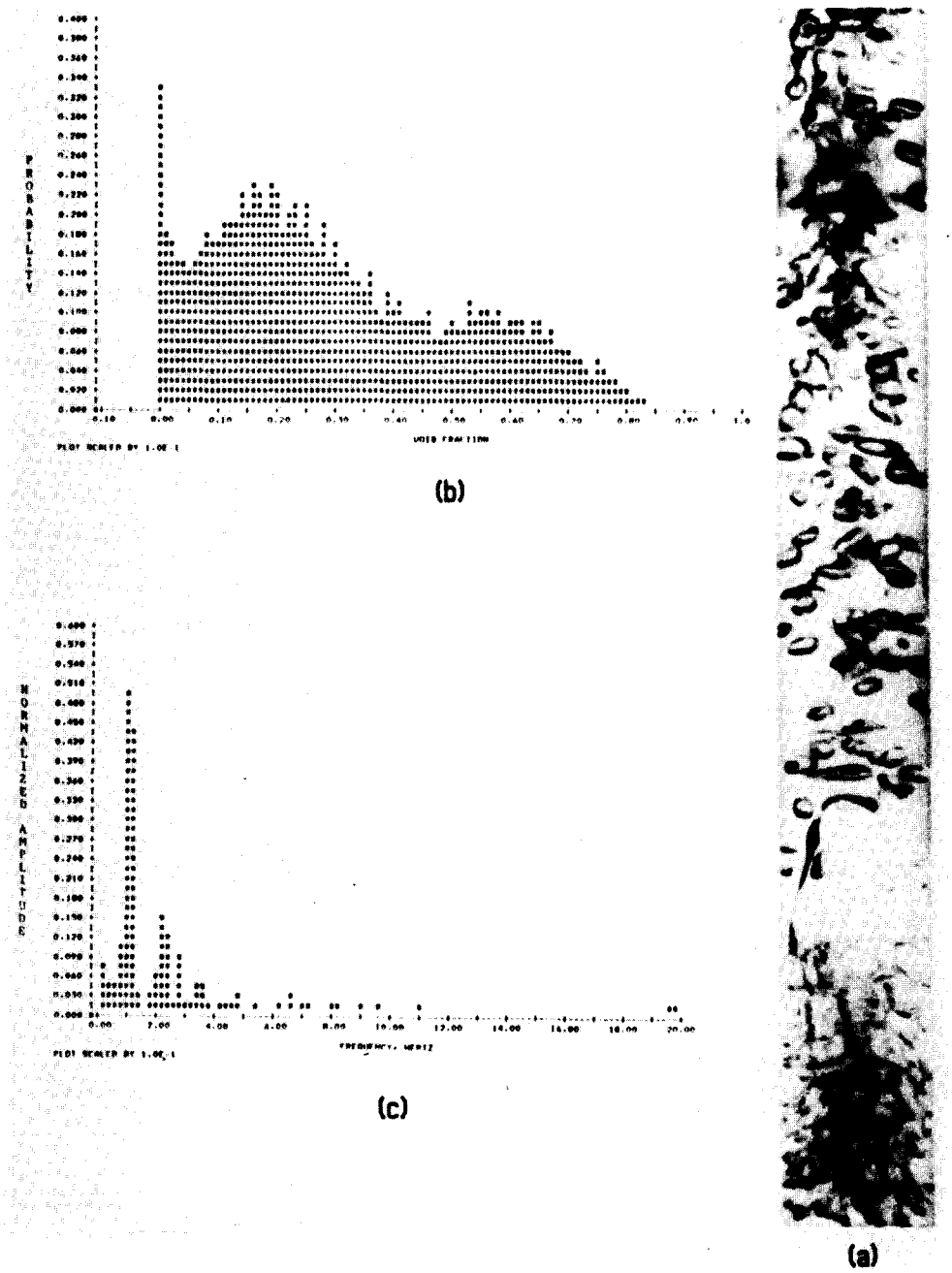

Figure 10. A photograph (a), diameter PDF (b), and diameter PSD (c), for 26 percent area-averaged void fraction, $j_L = 0.12$ m/sec, $j_G = 0.075$ m/sec.

slug-annular transition (at 70–80 percent chordal void fraction) is indicated since the variance changes sharply for a slight increase in void fraction. The curves then tend towards zero as the void fraction approaches either zero or one. This should be expected since the mean void fraction would be centered about zero or unity for a liquid filled or empty pipe, respectively. A discontinuity in the slope of the variance can be noted at about 0.4. This is interesting, since, as will be shown later, this agrees with the slug-annular transition seen in visual observations.

Two-phase flow structure can be readily associated with variance. Liquid bridging across the pipe is the primary physical difference between slug and annular flow. For slug flow, the presence of a low void region, associated with the liquid slug and entrained bubbles, and a high void region associated with the large spherical cap bubbles, produces considerable variance

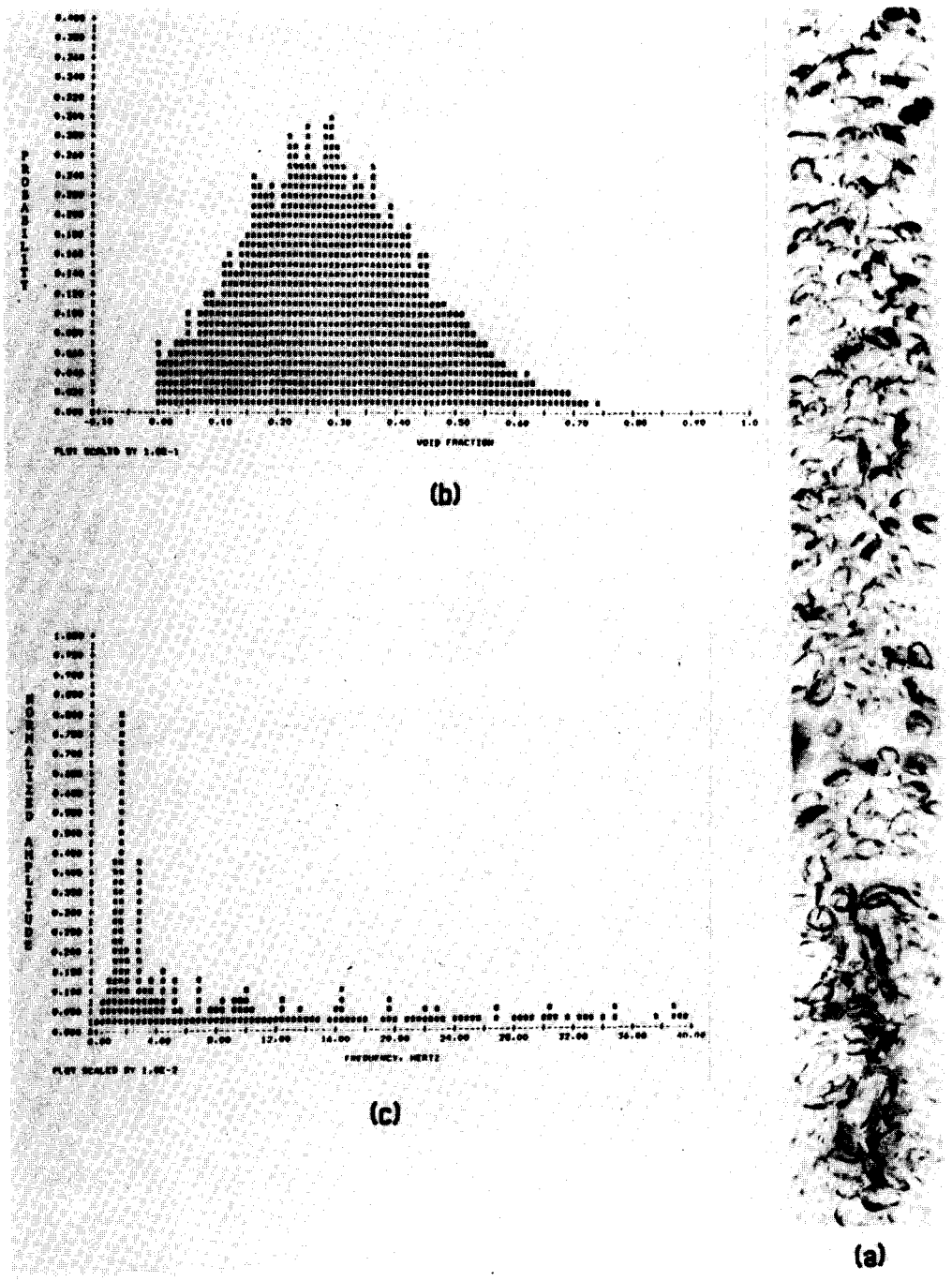

Figure 11. A photograph (a), diameter PDF (b), and diameter PSD (c), for 26 percent area-averaged void fraction, $j_L = 0.12$ m/sec, $j_G = 0.111$ m/sec.

from the mean. The disappearance of the liquid slug corresponds to a significant decrease in variance and thus indicates transition to annular flow.

A plot of the third moment, the coefficient of skewness, as a function of chordal void fraction is shown in figure 22. The skewness is relatively smooth in the bubbly-slug transition region, further indicating the smoothness of this occurrence. A potential slug-annular transition is indicated near 80 percent chordal-average void fraction. It can be seen that the skewness is relatively independent of position except for the wall measurement.

The fourth moment, the coefficient of kurtosis, is plotted as a functon of chordal-average

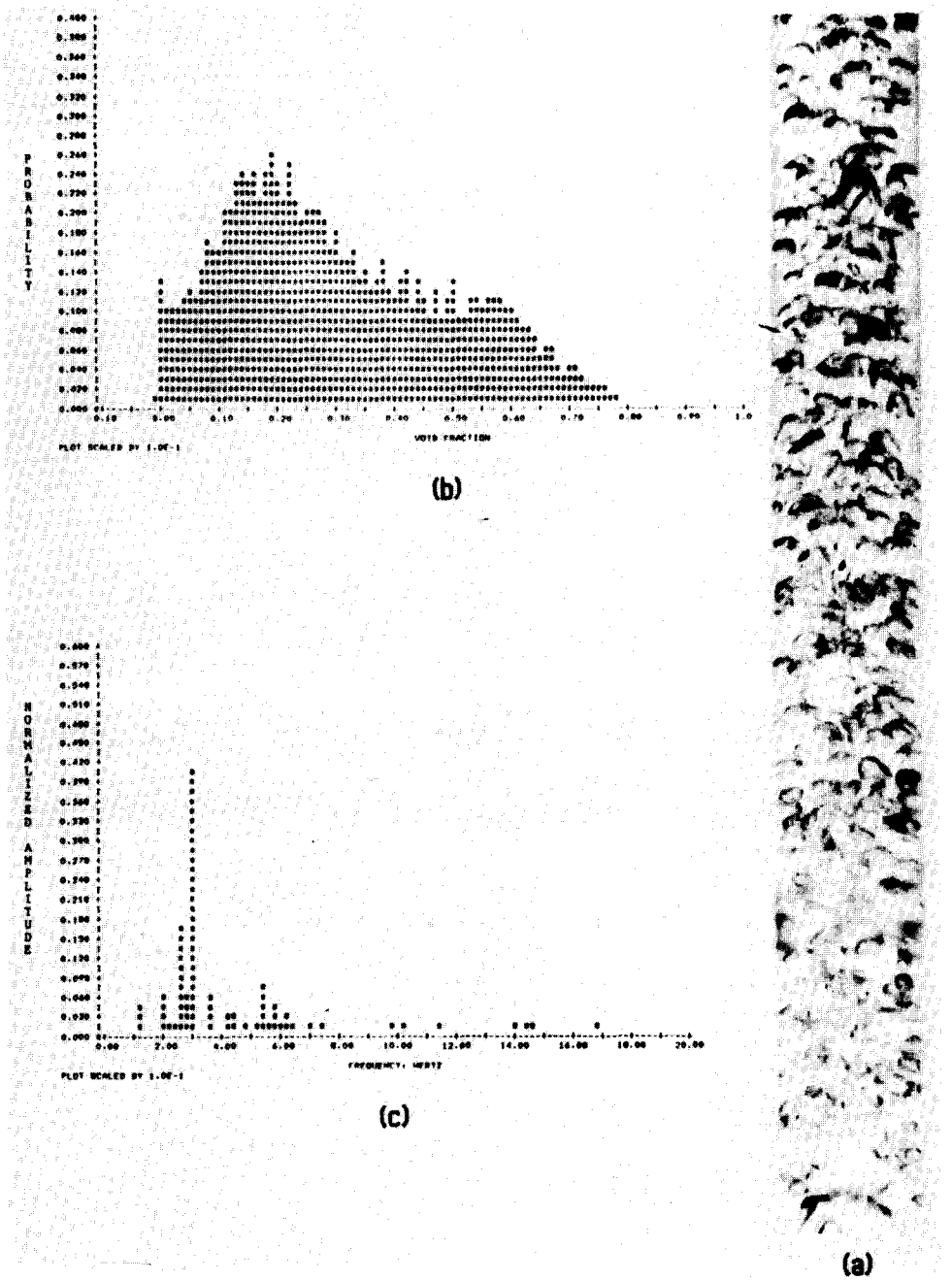

Figure 12. A photograph (a), diameter PDF (b), and diameter PSD (c), for 26 percent area-averaged void fraction, $j = 0.25$ m/sec, $j_G = 0.177$ m/sec.

void fraction in figure 23. This parameter is also constant in the bubbly-slug transition region.

The kurtosis, like the lower moments, indicates flow regime transition near 80 percent chordal-average void fraction. This response corresponds to a substantial increase in peakedness caused by the disappearance of the liquid slugs. It should be noted that measurements made near the wall, i.e., the '*E*' and '*F*' chords, do not exhibit the same trends as data acquired elsewhere.

3.1.2.2 *Non-zero liquid flow data.* Any practical flow regime indicator should be independent of fluid velocity. Thus, the data acquired at non-zero liquid flows was compared to that acquired at zero liquid flow.

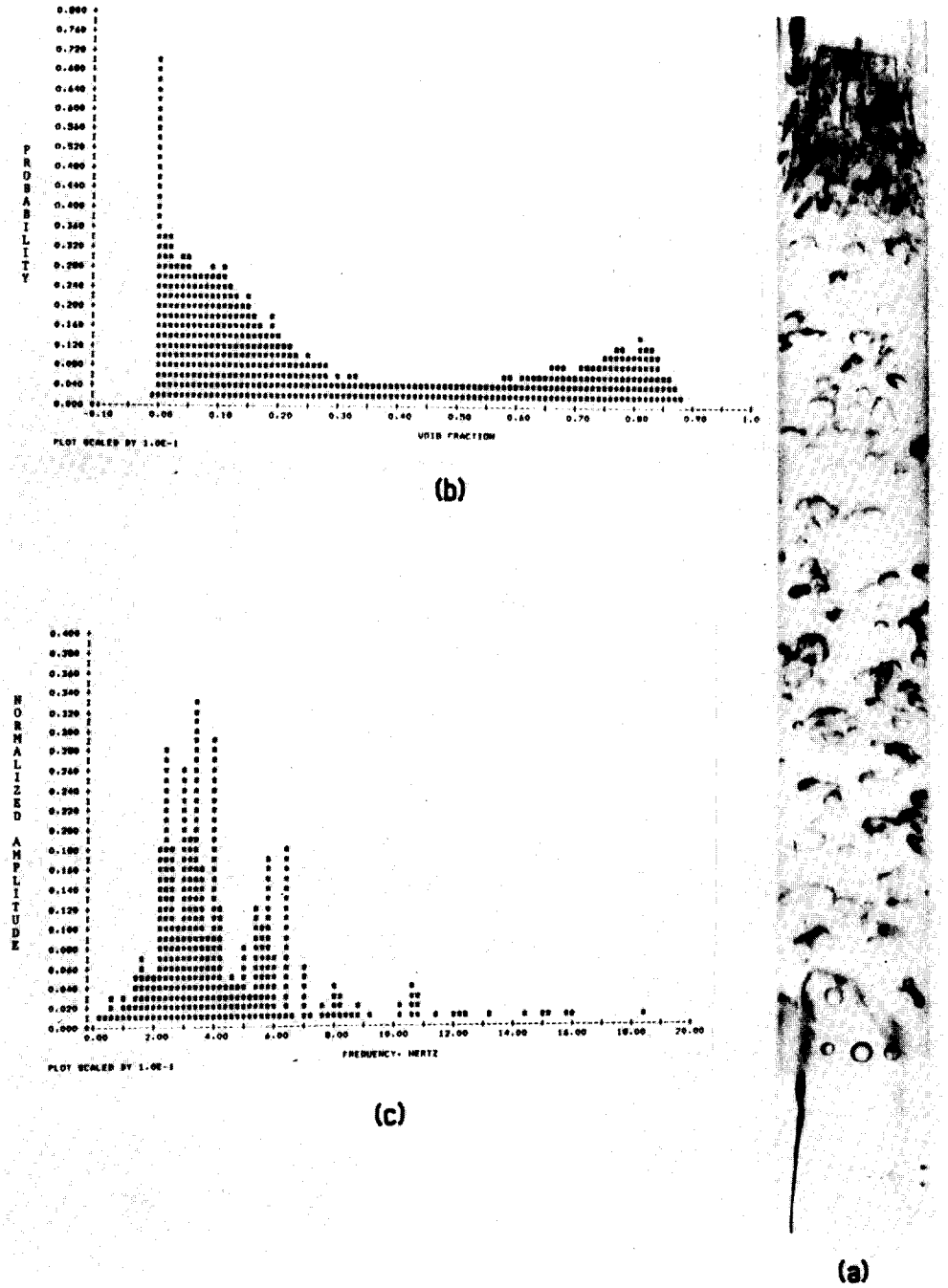

Figure 13. A photograph (a), diameter PDF (b), and diameter PSD (c), for 26 percent area-averaged void fraction, $j_L = 0.37$ m/sec, $j_G = 0.257$ m/sec.

The variance was observed to be relatively constant in bubbly flow. The variance initially decreases with the onset of liquid velocity. This occurrence indicates that the bubbly-slug transition is surpressed by the liquid velocity. A further increase in liquid velocity cannot stop the transition back to slug flow because of the corresponding increase in vapor flow rate necessary to maintain constant area-averaged void fraction. This phenomena is shown in figure 24 at 26 percent area-averaged void fraction. Notice that all non-wall chords indicate similar trends. Clearly, the bubbly-slug flow regime transition does not occur at constant void fraction, however it was found that a variance of 0.04 also predicts the visually observed bubbly-slug transition.

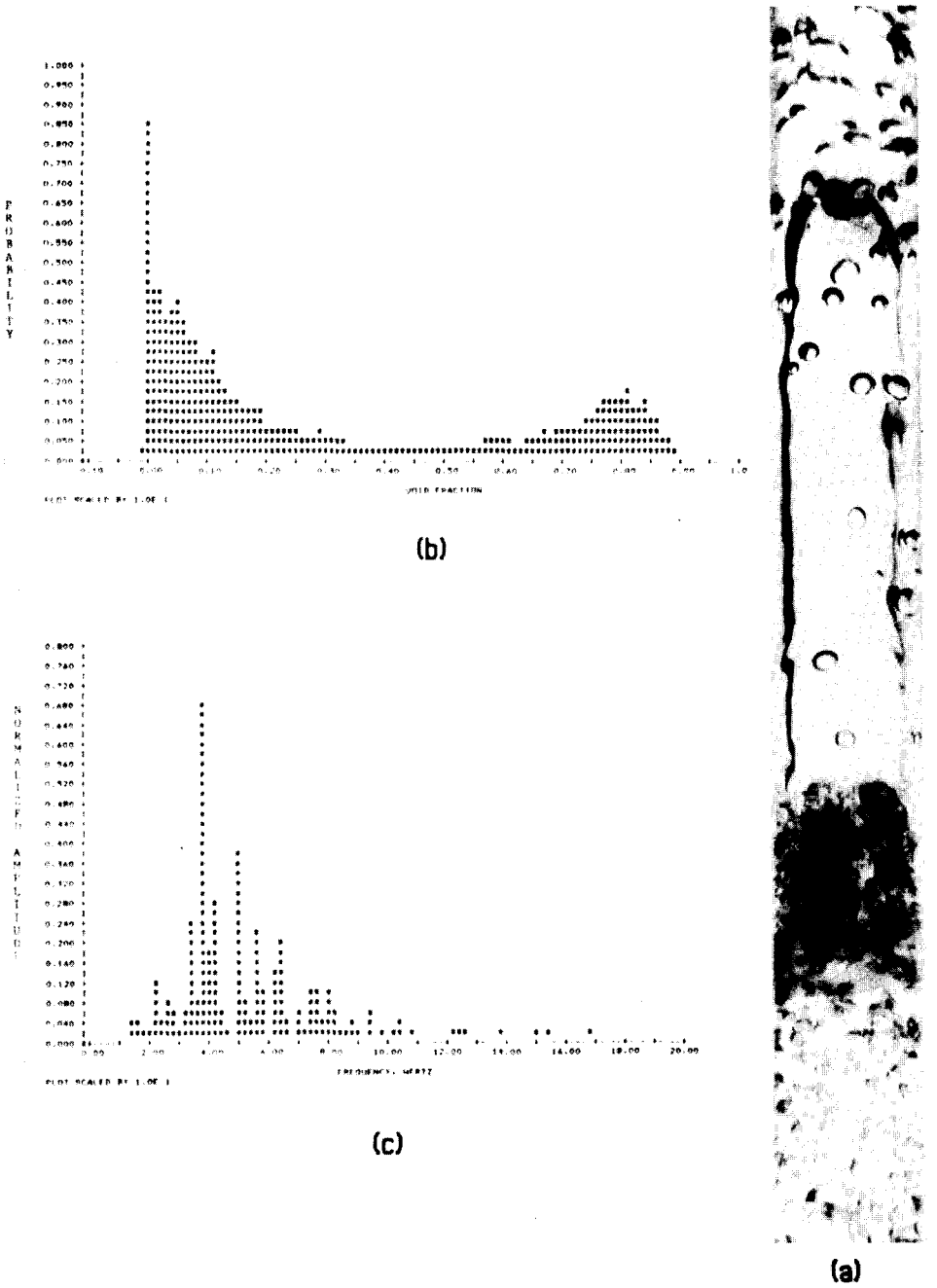

Figure 14. A photograph (a), diameter PDF (b), and diameter PSD (c), for 26 percent area-averaged void fraction, $j_L = 0.50$ m/sec, $j_G = 0.329$ m/sec.

Figure 25 illustrates the variance as a function of liquid superficial velocity at 68 percent area-averaged void fraction. A monotonic decrease in variance is observed as the liquid velocity increases. The large vapor flow rates associated with this void fraction tend to force the liquid to the wall enhancing a slug-annular transition.

The shape of the skewness versus liquid superficial velocity graph is similar to the same corresponding graph for the variance, however, the magnitude of the skewness does not change in a fashion necessary to establish a precise bubbly-slug flow regime indicator. Th magnitude of the skewness generally decreases with increasing void fraction, however, a transition from bubbly to slug flow produces an increase in skewness. These two phenomena occur simultaneously and tend to offset each other.

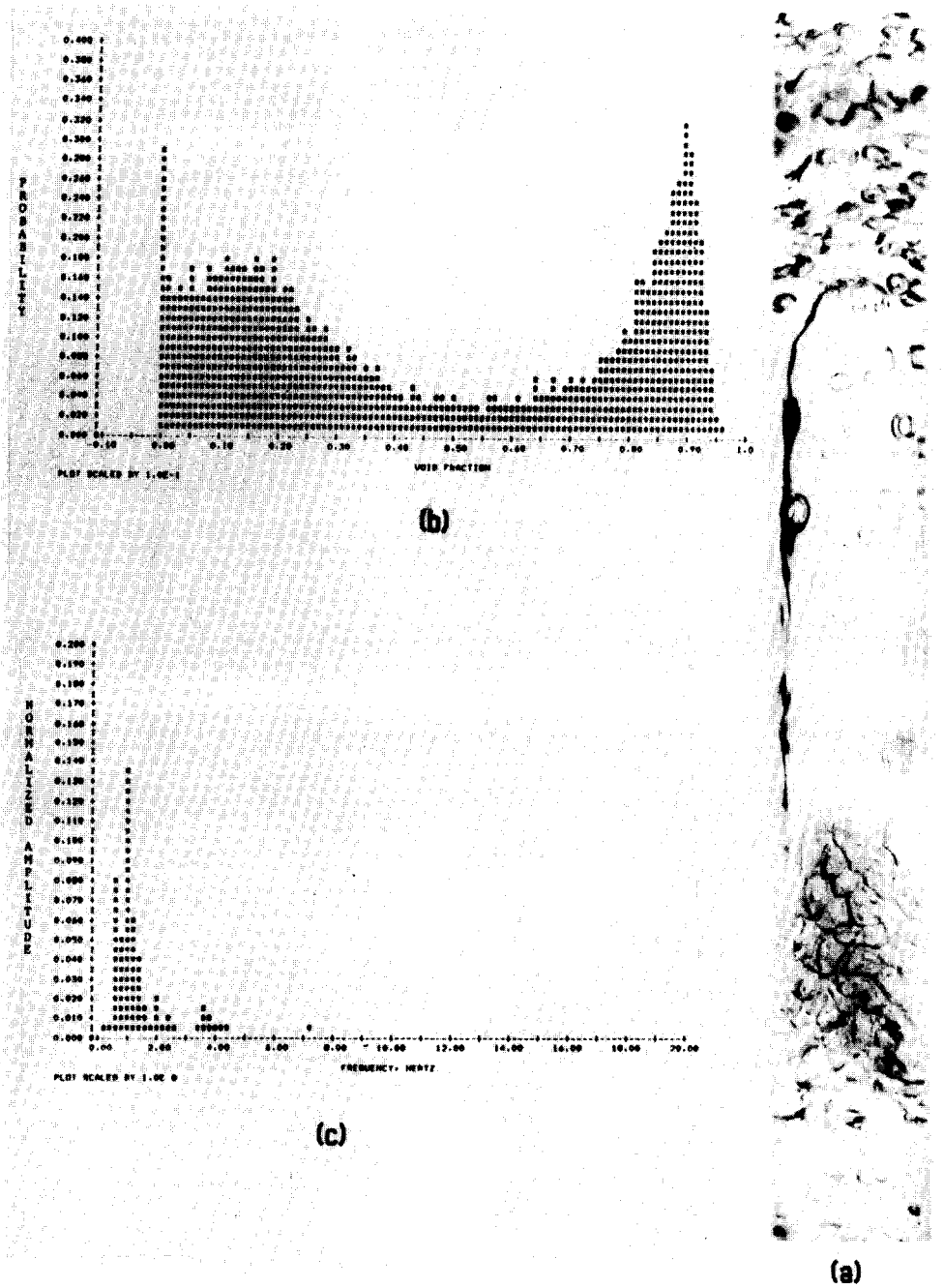

Figure 15. A photograph (a), diameter PDF (b), and diameter PSD (c), for 41 percent area-averaged void fraction, $j_L = 0.0$ m/sec, $j_G = 0.184$ m/sec.

Kurtosis, the fourth moment about the mean, is quite independent of liquid velocity and correspondingly flow regime. The coefficient of kurtosis is invariant with respect to liquid superficial velocity for area-averaged void fractions of 13, 20 and 26 percent. The magnitude of the coefficient of kurtosis does change as a function of voidage and is relatively independent of position. Thus a bubbly-slug flow regime indicator is not possible using the coefficient of kurtosis.

In the slug flow regime, the coefficient of kurtosis again does not exhibit any dependence on liquid superficial velocity. Moreover, the coefficient of kurtosis is independent of chordal position.

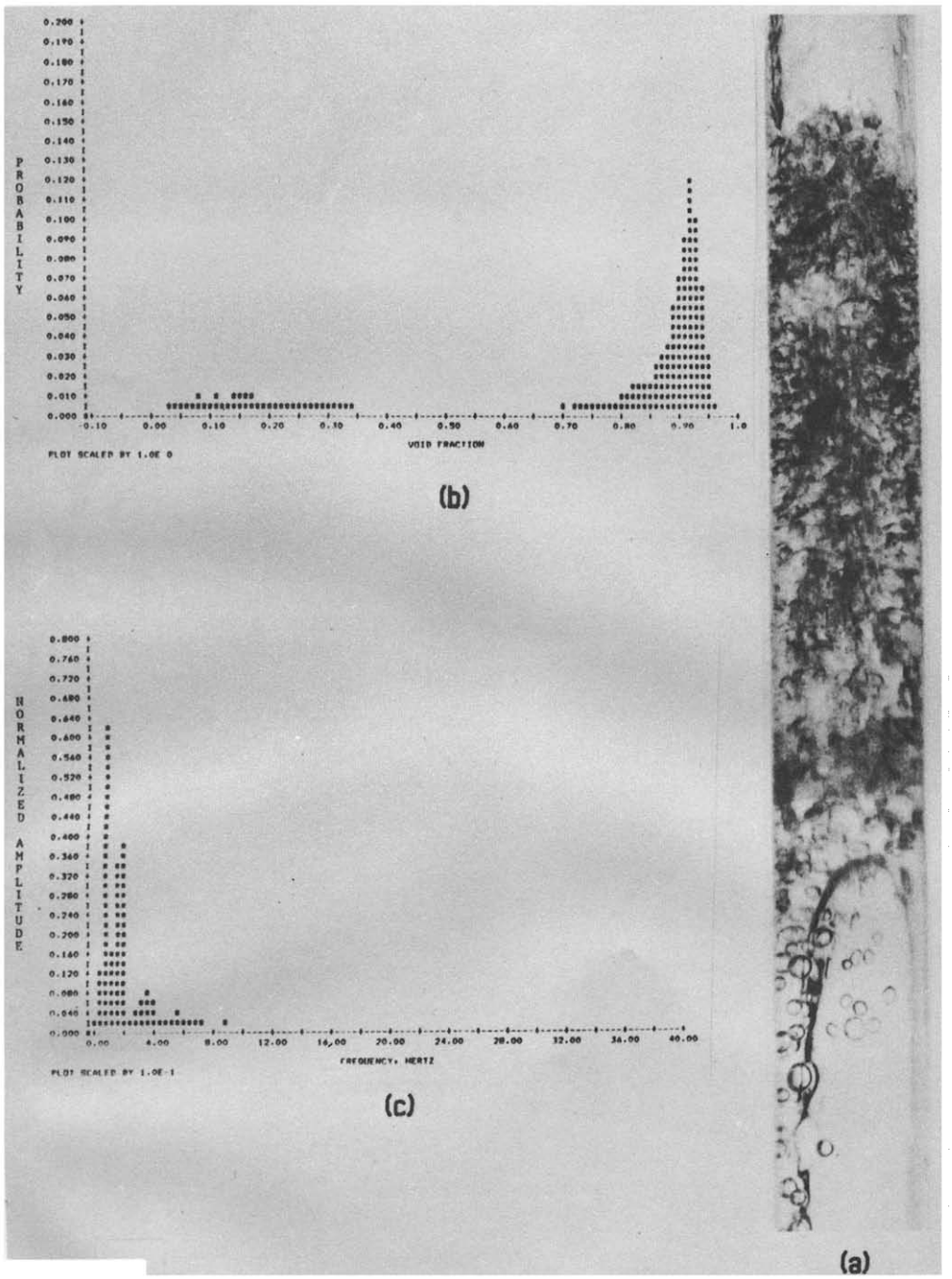

Figure 16. A photograph (a), diameter PDF (b), and diameter PSD (c), for 68 percent area-averaged void fraction, $j_L = 0.0$ m/sec, $j_G = 0.981$ m/sec.

A further increase in void fraction results in considerable variation in the coefficient of kurtosis as a function of chordal position. Superficial liquid velocity effects were also observed. These trends are expected since the kurtosis is a measure of the distribution's peakedness. Around the slug-annular transition, the void distribution is more peaked for the chord along the diameter than the one adjacent to the wall.

3.1.3 Power spectral density (PSD) data. Three types of power spectra were observed:

(1) A wide band, low amplitude spectrum, usually associated with bubbly flows.

(2) A low frequency peak of large amplitude, usually associated with the characteristic frequency of slug flow.

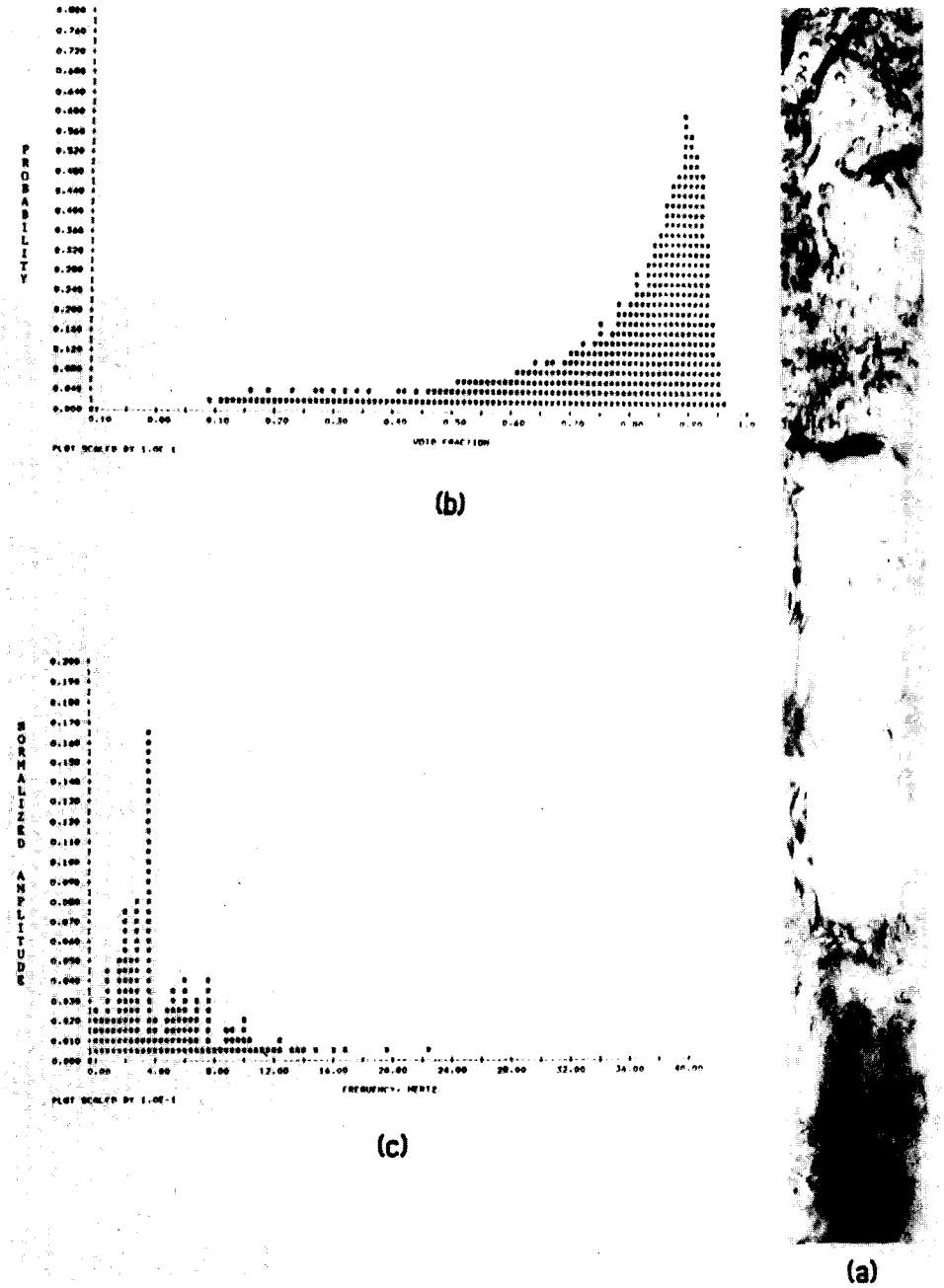

Figure 17. A photograph (a), diameter PDF (b), and diameter PSD (c), for 68 percent area-averaged void fraction, $j_L = 0.12$ m/sec, $j_G = 1.67$ m/sec.

(3) A medium width band with an amplitude spectrum corresponding to annular flow.

The band width of the bubbly flow spectrum will increase with liquid velocity since the shorter void transit time corresponds to higher frequencies. Similarily, the PSD for slug flow shifts to high frequency as the liquid superficial velocity is increased. Annular flow is composed of the frequencies of the liquid film thickness variation and roll waves moving along the liquid film /vapor interface, and thus produces a spectrum of medium width, which increases with liquid velocity.

All moments associated with the PSD exhibit a strong dependence on superficial liquid velocity. This characteristic is very undesirable for a flow regime indicator because any correlation would require knowledge of the liquid superficial velocity. Void fraction measure-

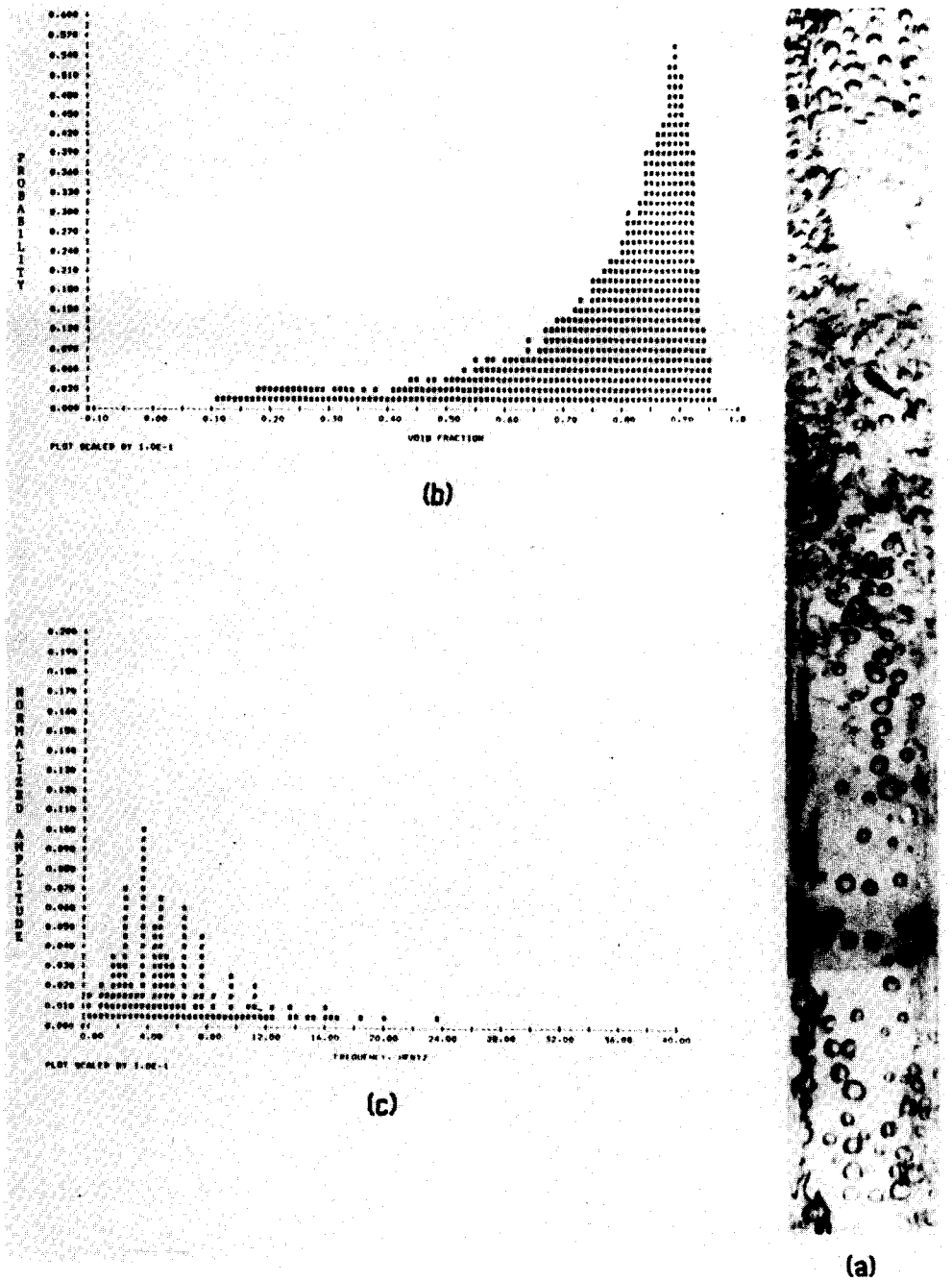

Figure 18. A photograph (a), diameter PDF (b), and diameter PSD (c), for 68 percent area-averaged void fraction, $j_L = 0.25$ m/sec, $j_G = 2.67$ m/sec.

ments are sufficiently difficult, the requirement of a simultaneous liquid velocity measurement renders the use of PSD moments impractical. Moreover, only the variance of the PSD has possibilities for a flow regime indicator. The skewness and kurtosis are essentially independent of the flow regime. As a result, the moments of the PSD are not considered to be as valuable as the moments of the PDF for flow regime identification.

3.2 *Data consistency*

Several verifications were performed to assure data accuracy. A statistically stationary and ergotic process was shown to exist (Vince & Lahey 1980); thus, the moments computed from the PSD and PDF are representative of the phenomena being measured.

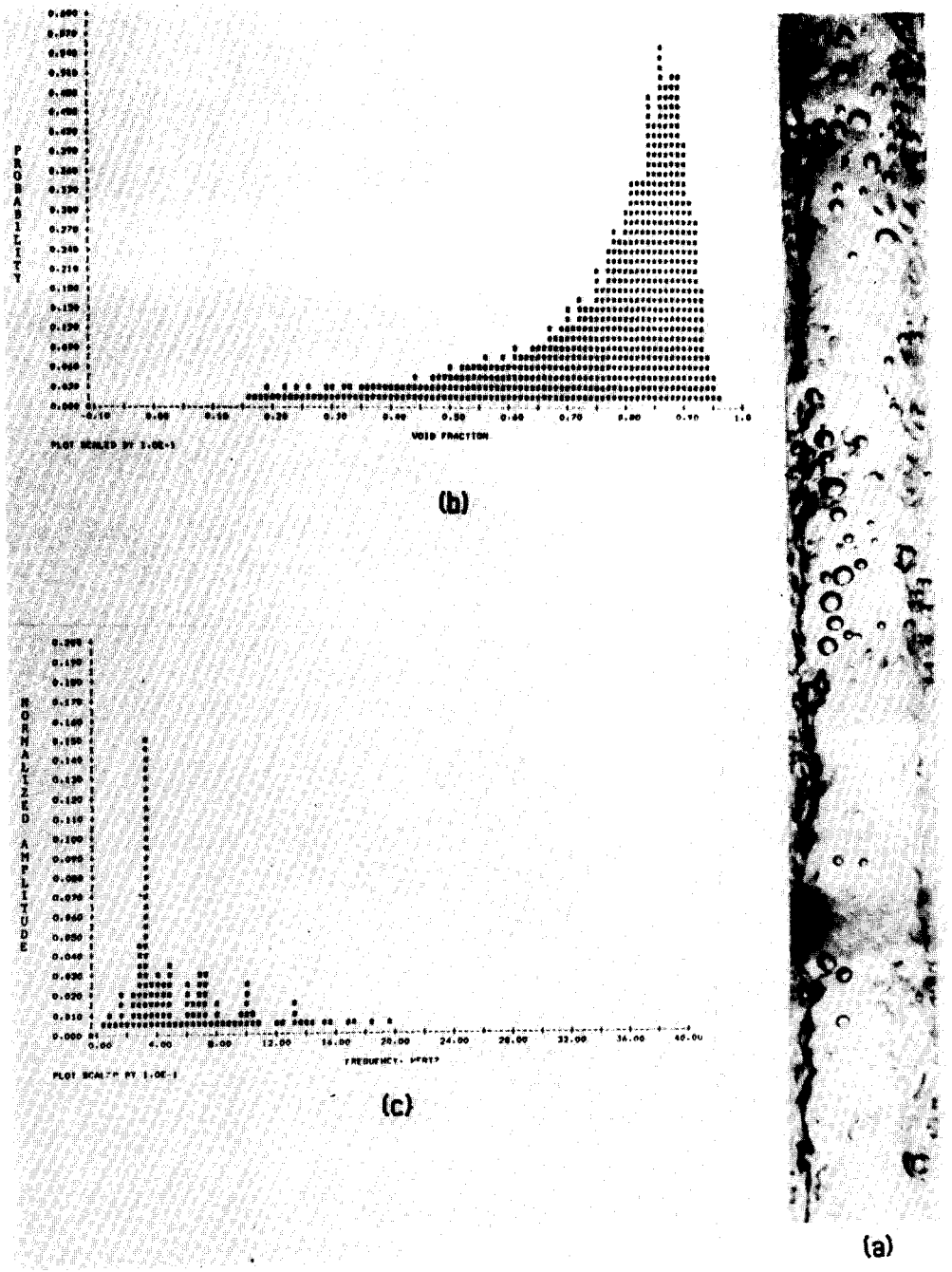

Figure 19. A photograph (a), diameter PDF (b), and diameter PSD (c), for 68 pecent area-averaged void fraction, $j_L = 0.37$ m/sec, $j_G = 3.41$ m/sec.

Another verification was obtained by comparing the global void fraction, determined from simultaneous pressure drop measurements, with the integrated chordal X-ray measurements (i.e. the area-average void fraction). Due to the low velocities studied, the frictional pressure drop is very small. A differential pressure measurement will then produce an accurate estimate of the global void fraction. An appropriate integration scheme was proposed previously by Pike *et al.* (1965). The results are shown in figure 26. Considering that inherent fluctuation in system pressure drop made an accurate monometer reading difficult (particularly for the slug flow regime), the observed agreement is quite good.

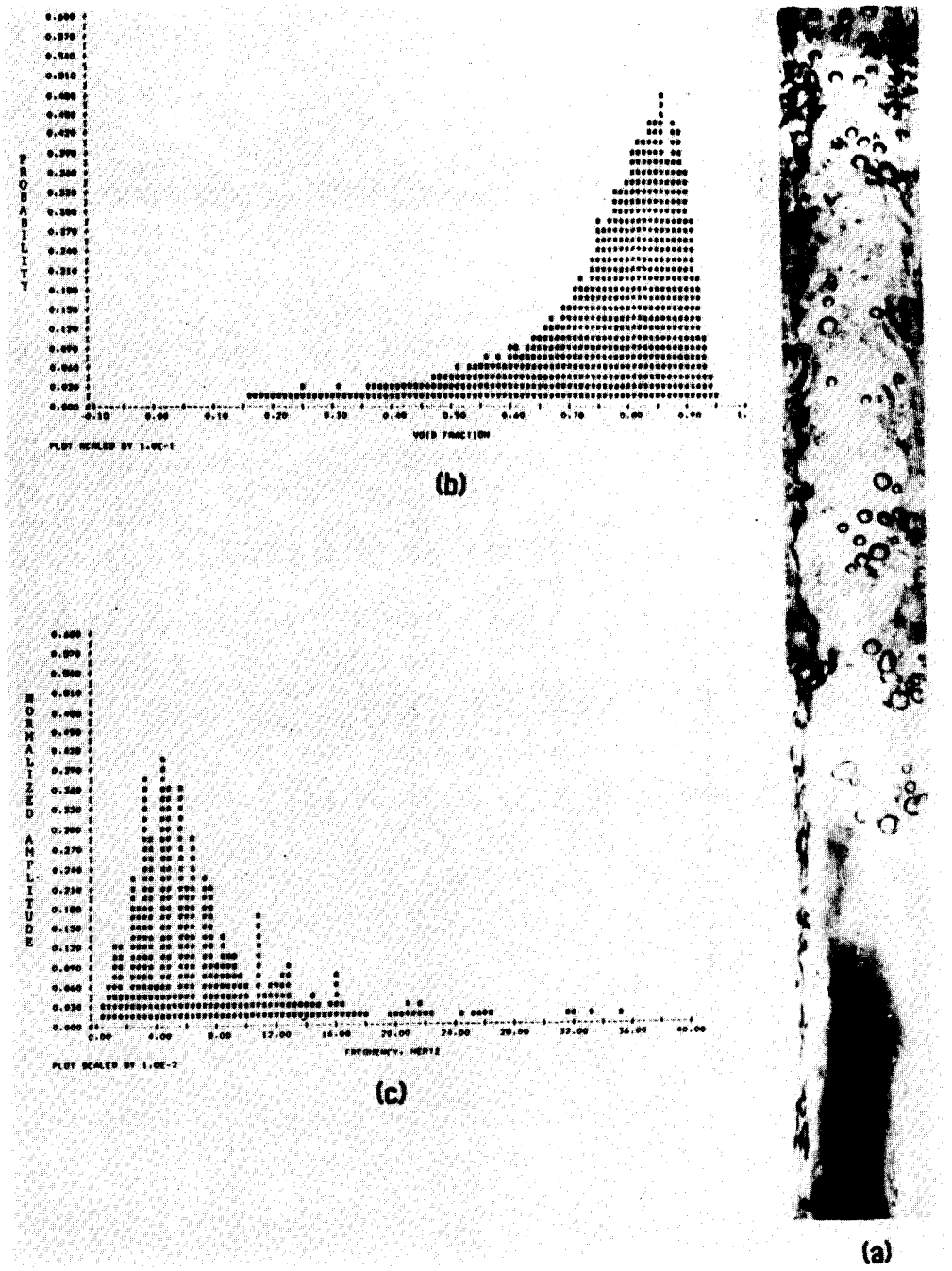

Figure 20. A photograph (a), diameter PDF (b), and diameter PSD (c), for 68 percent area-averaged void fraction, $j_L = 0.50$ m/sec, $j_G = 4.24$ m/sec.

3.3 *Comparisons with other data*

Zuber & Findlay (1965) have previously presented a correlation for the vapor phase velocity and the mixture superficial velocity ($\langle j \rangle$). They found that plotting data in the $\langle j_g \rangle / \langle \alpha \rangle$ vs$\langle j \rangle$ plane produces a straight line with a slope of C_0, the void concentration parameter, and a y-intercept of V_{gj}, the drift velocity. It has been previously shown (Zuber & Findlay 1965) that the C_0 parameter can range from 1.0 to 1.6, depending on the fluid system pressure and geometry, and v_{gj} can vary from 0.3 to 1.2 ft/sec. Our flow and void fraction data were combined to produce a plot in the so called "Zuber–Findlay" plane. This graph, shown in figure 27, indicates that our data is correlated by a C_0 of 1.29 and a V_{gj} of 0.15 m/s. A least squares fit of the data produces a correlation coefficient of 0.999 (i.e. near perfect correlation). Obviously, these values are well

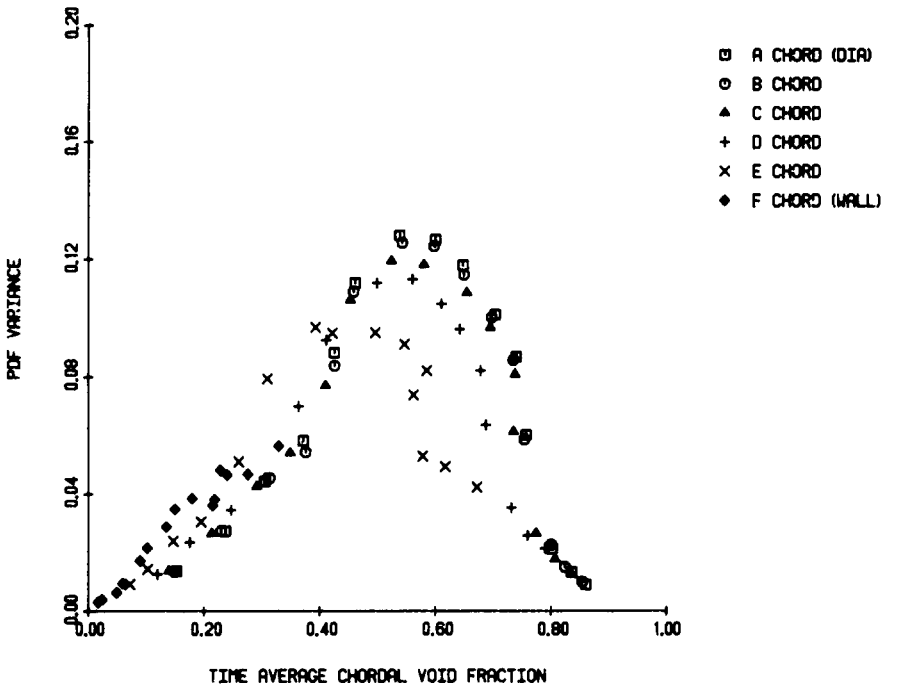

Figure 21. The PDF variance vs time average chordal void fraction for $j_L = 0.0$ m/sec.

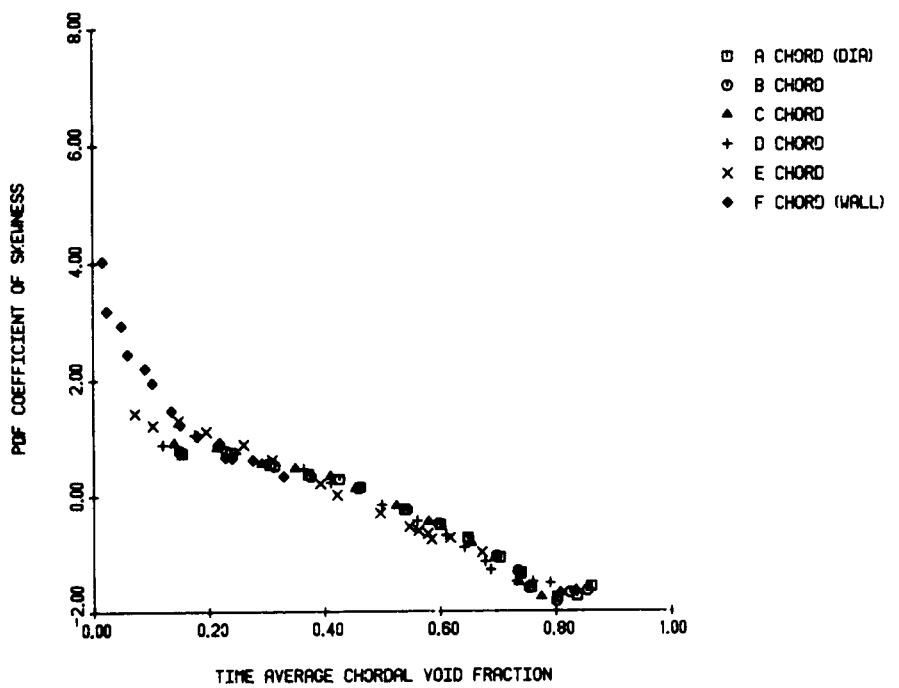

Figure 22. The PDF coefficient of skewness vs time average chordal void fraction for $j_L = 0.00$ m/sec.

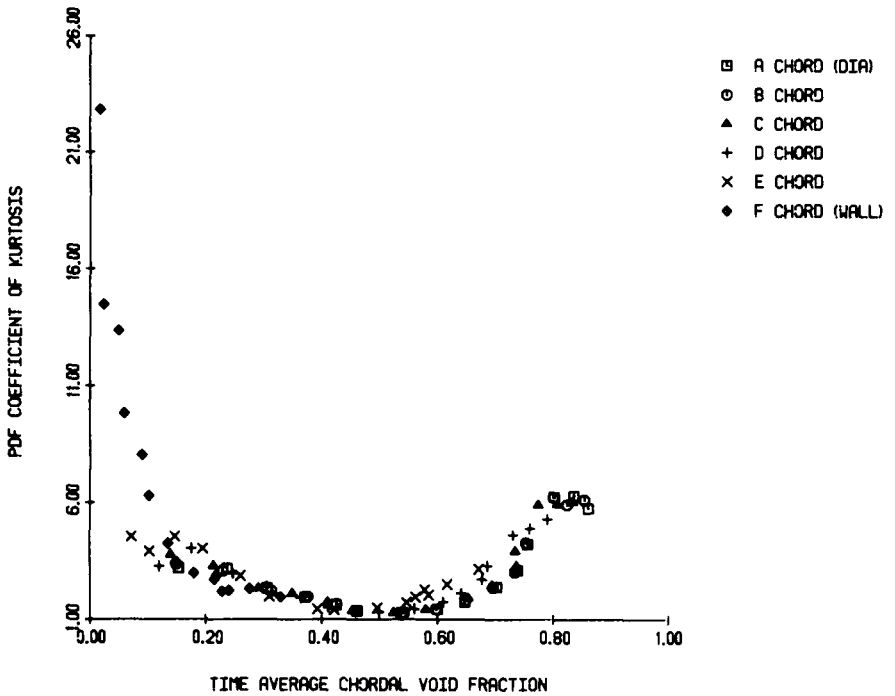

Figure 23. The PDF coefficient of kurtosis vs time average chordal void fraction for $j_L = 0.00$ m/sec.

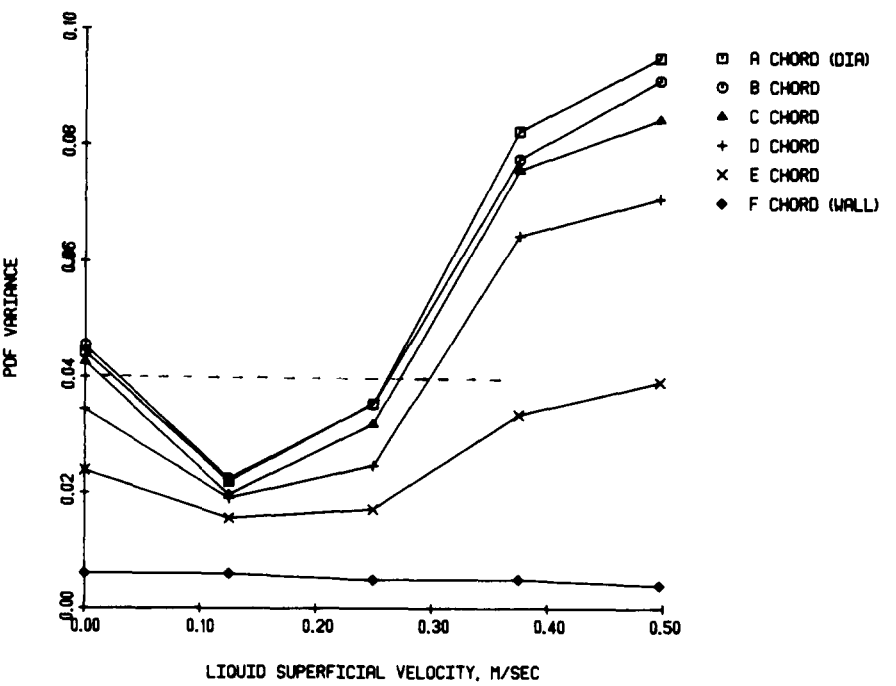

Figure 24. The PDF variance vs superficial liquid velocity at 26 percent area-averaged void fraction.

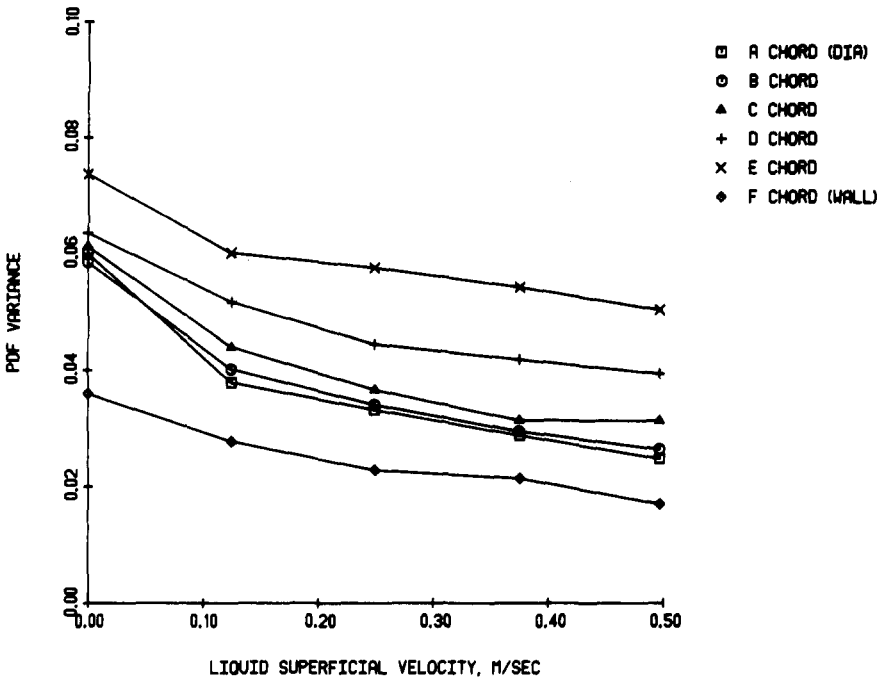

Figure 25. The PDF variance vs superficial liquid velocity at 68 percent area-averaged void fraction.

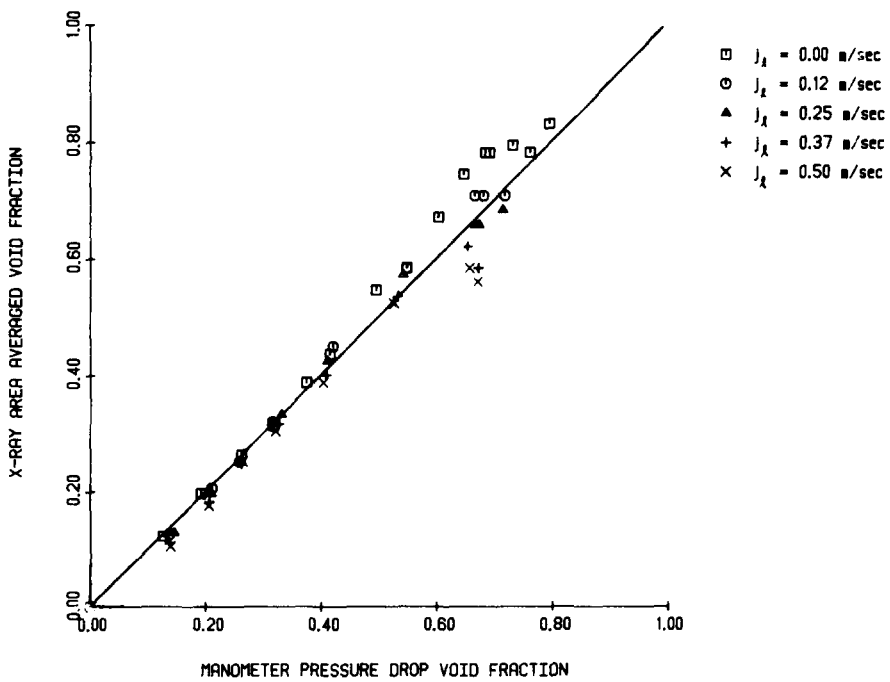

Figure 26. X-ray area-averaged vs manometer pressure drop void fraction.

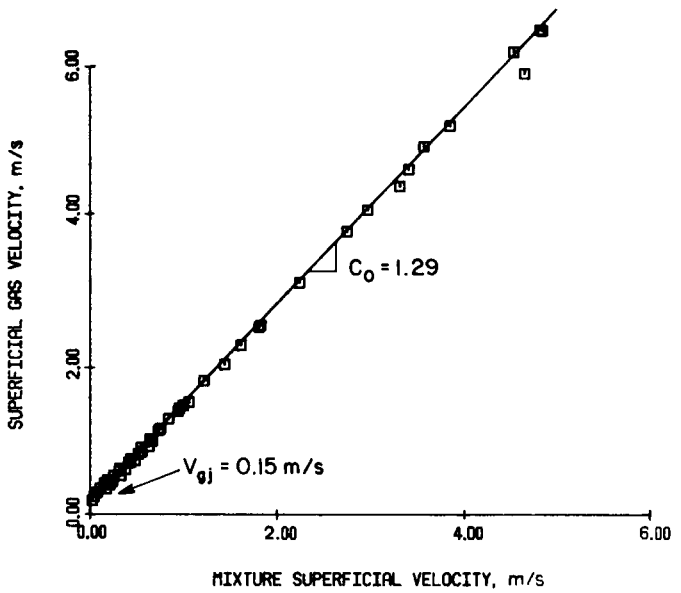

Figure 27. The RPI X-ray data in the Zuber–Findlay (1965) plane.

within the ranges indicated by Zuber & Findlay (1965). Since reasonable agreement with similar previous works, and independent measurements, was achieved, the X-ray data presented herein is believed to be accurate.

3.4 *Recommended flow regime indicator*

The moments of the PDF and PSD associated with a variety of two-phase conditions were calculated. Even though flow regime information is evident in many of the moments calculated, the PDF variance, or second moment about the mean, appears to be the best flow regime indicator. For the pipe flow data analyzed, a variance greater than 0.04 indicated slug flow. Smaller variances indicate a bubbly or annular flow regime, depending on the mean void fraction. This flow regime indicator is not strongly dependent on the superficial liquid velocity, and is fairly independent of chordal measurement position, thus it appears to be a good choice.

The flow regime map determined using this criterion is shown in figure 28. Comparing this figure with the flow regime boundaries indicated in figure 6 (developed from direct visual observations), we see that the 0.04 variance criterion proposed does a good job.

This flow regime map disagrees somewhat with other maps. Figure 29 compares the results shown in figure 28 with the map suggested by Taitel & Dukler (1980). It can be seen that the bubbly-slug (i.e. churn) transition boundary is in good agreement however the slug-annular transition is off significantly. This may be fortuitous since their flow regime criteria for the bubbly-slug flow regime transition is based on a constant area-averaged void fraction, a trend which was not observed in this study. Moreover, their slug-annular transition criterion of 15 m/sec is not supported by our data.

As shown in figure 30, our 0.4 variance flow regime indicator produces reasonable agreement with Griffith & Wallis (1961) map for the slug-annular transition. It also agrees with the Griffith and Wallis flow regime map for data acquired at zero liquid flow for the bubbly-slug transition. However a significant discrepancy exists at the bubbly-slug transition for non-zero liquid flow.

Duns & Ros (1963) also proposed a flow regime map. The variance criterion proposed herein disagrees with this map as shown in figure 31. Duns & Ros predict the existence of bubbly flow when slug flow was visually observed and indicated by the 0.04 variance criterion. Likewise, Duns & Ros predict slug flow when annular flow was observed and predicted by our criterion.

The map proposed by Govier & Aziz (1972) is in better agreement but, as shown in figure 32, still differs somewhat from the 0.04 variance criterion prediction for the bubbly-slug transition.

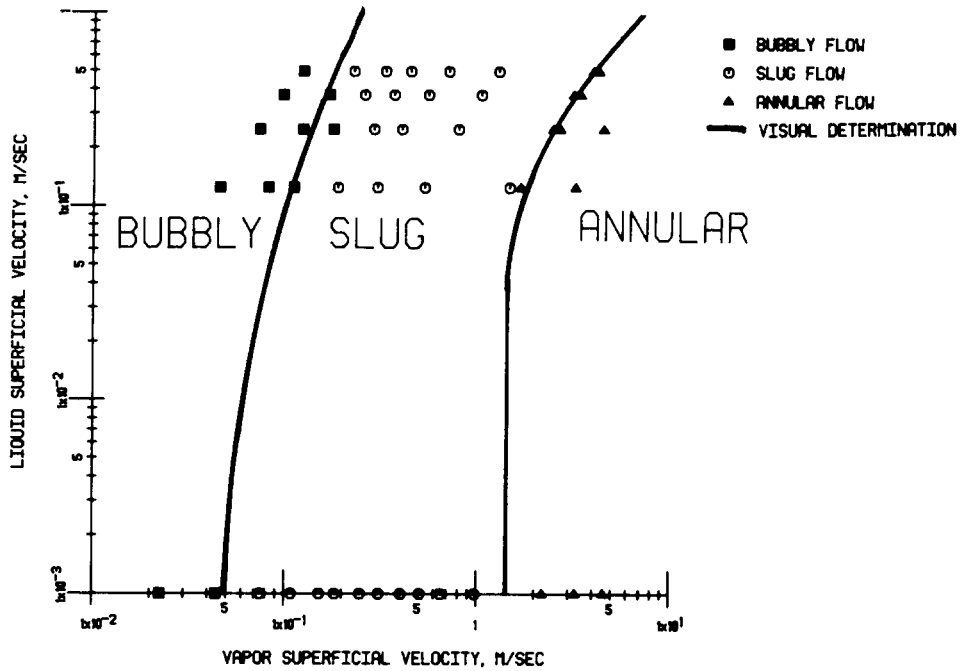

Figure 28. A flow regime map based on a PDF variance of 0.04.

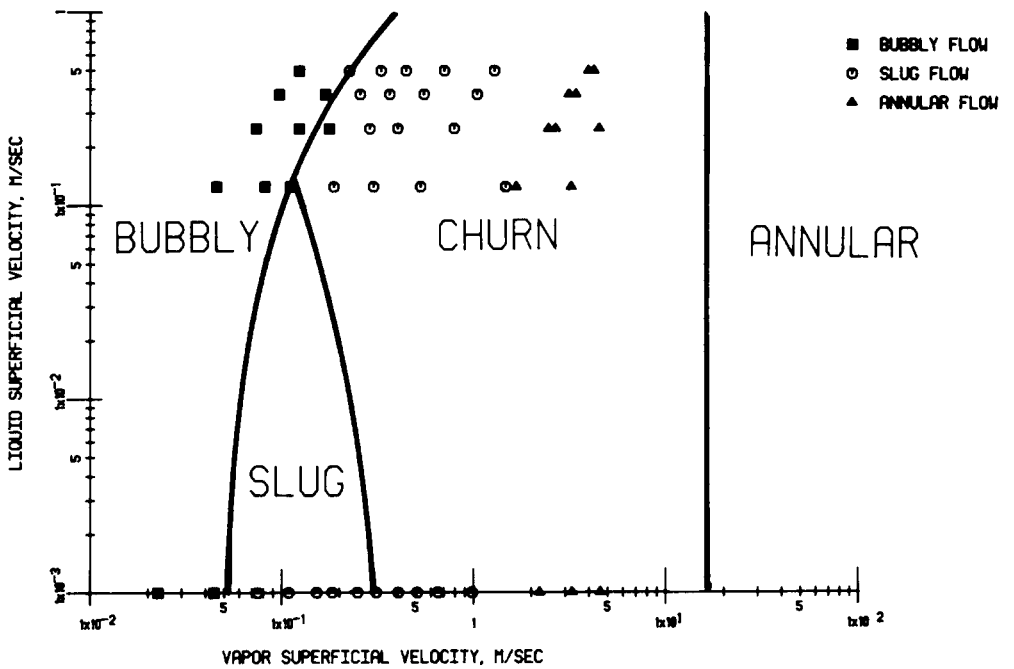

Figure 29. A comparison of the RPI X-ray data and Taitel & Dukler (1980) correlations.

It should be noted that the maps suggested by earlier researchers do not completely agree amongst themselves, thus it is no surprise that our data does not agree with all of them. Indeed, this disagreement is a reflection of the subjective nature of previous investigators' flow regime maps, and clearly indicates the need for an objective criterion.

It should be stressed that our data base is limited to low pressure air/water flow in circular conduits, and thus the generality of using a constant PDF variance (i.e. 0.04) as a flow regime transition criterion needs further verification. Nevertheless, it appears to be a very promising criterion.

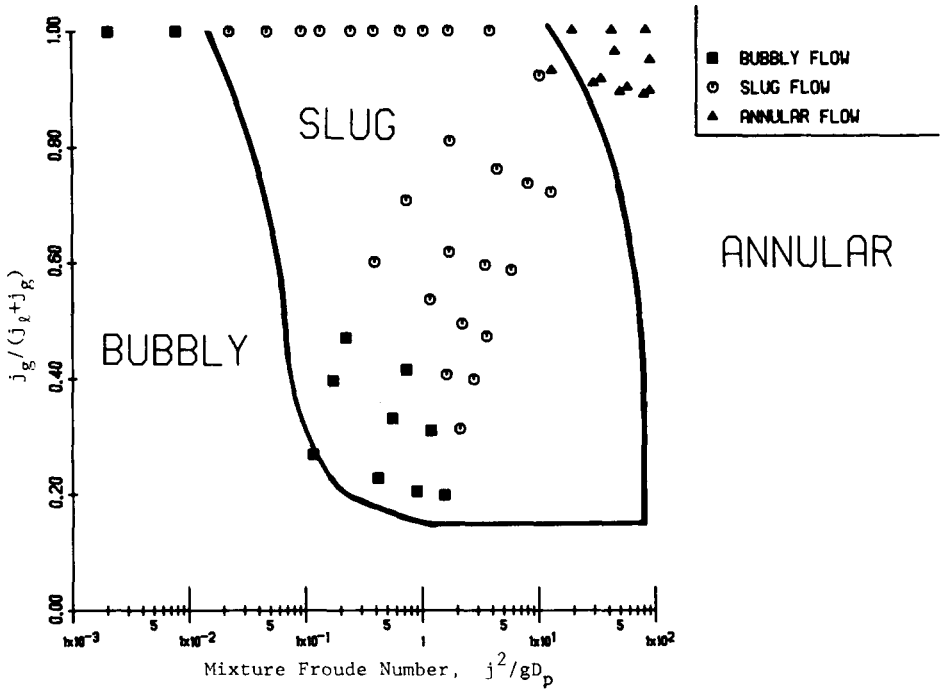

Figure 30. A plot of the RPI X-ray data on the coordinates suggested by Griffith & Wallis (1961).

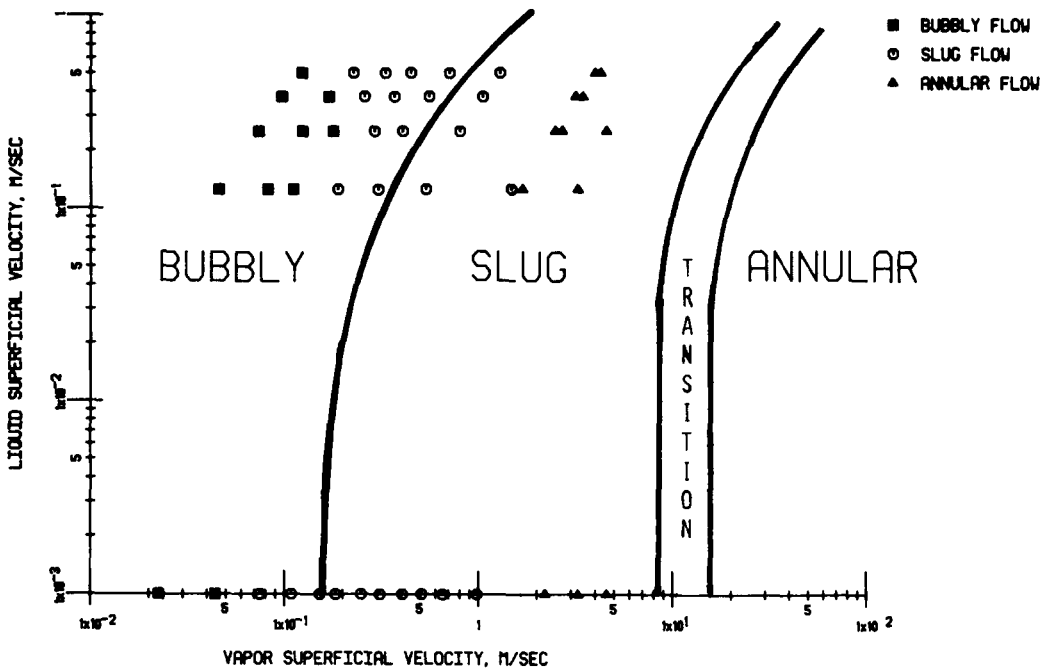

Figure 31. A comparison of the RPI X-ray data and the flow regime map proposed by Duns & Ros (1963).

4. SUMMARY AND RECOMMENDATIONS

4.1 *Flow regime identification*

Forty-nine two-phase flows were studied with a dual beam X-ray system. The chordal void fraction was measured at six chordal locations across the pipe for each low pressure air/water flow. The probability density function (PDF) and power spectral density (PSD) function, and their first four moments, were calculated for each chordal position.

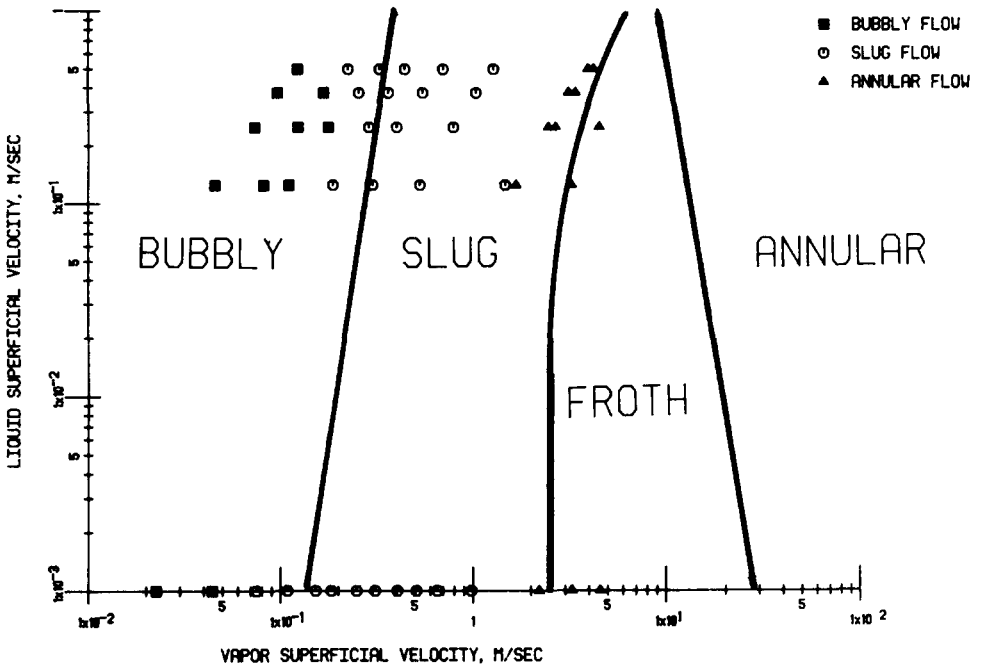

Figure 32. A comparison of the RPI X-ray data and the flow regime map proposed by Govier & Aziz (1972).

An objective flow regime indicator was developed from the first four moments associated with the PDF and PSD. The variance of the PDF is recommended. This moment responded to the observed changes in flow regime and was found to be independent of liquid superficial velocity. For the conditions tested in this study the level of variance which indicated the bubbly-slug and slug-annular flow regime transition was found to be 0.04, independent of flow rate. Clearly, more work needs to be done to further investigate this technique in complex geometries, and at higher pressures. Nevertheless, the technique appears quite promising for further development.

The moments of the PSD need to be correlated with liquid superficial velocity in order to be useful. This would require the simultaneous measurement of the liquid superficial velocity. Thus the PSD, and its moments, are not recommended as objective flow regime indicators.

Finally, it was observed that the commonly used flow regime transition criterion of a constant void was inadequate.

Acknowledgement—The authors wish to acknowledge the financial support given this study by Dr. Y. Y. Hsu under USNRC Contract NRC-04-76-301.

NOMENCLATURE

A_d detector area intersected by photon beam, cm^2
C chord length through two-phase mixture, cm
C_{M_3} the coefficient of skewness
C_{M_4} the coefficient of kurtosis
f frequency, Hertz
$\mathrm{Im}(f, T_r)$ imaginary part of power spectral density as a function of frequency and record length, s^{-1}
I_0 photon intensity incident on test section, photons/cm^2-s
$I(x)$ unattenuated intensity at distance x into the media, photons/cm^2-s
M_2 variance

M_3 skewness
M_4 kurtosis
M_n nth moment about the mean
p_i probability of ith void fraction
PSD(f) normalized amplitude of power spectral density as a function of frequency, s
Re(f, T_r) real part of power spectral density as a function of frequency and record length, s^{-1}
R_G output voltage corresponding to all vapor ($\alpha = 1$)
R_L output voltage corresponding to all liquid ($\alpha = 0$)
R_{SD} source to detector distance, cm
R_{ST} source to test section distance, cm
$R(t)$ $\triangleq \ln(V_s^*(V_r^*))$ output voltage corresponding to instantaneous chordal void fraction
T wall thickness of conduit, cm
T_r record length, s
V_r^* signal (voltage) from the X-ray beam going through the reference attenuation
V_s^* signal (voltage) from the X-ray beam going through the test section
x thickness of attenuating media, cm
x_G vapor path length, cm
x_L liquid path length, cm

Greek symbols

α chordal-average void fraction
α_i the ith void fraction
ϵ detector efficiency
θ integration time
$\bar{\mu}$ average attenuation coefficient for two-phase mixture, cm^{-1}
μ_G vapor attenuation coefficient, cm^{-1}
μ_L liquid attenuation coefficient, cm^{-1}
μ_W attenuation coefficient of test section walls, cm^{-1}

REFERENCE

BENDAT, J. S. & PIERSOL, A. G. 1971 *Random Data: Analysis and Measurement Procedures*, pp. 326–327. Wiley-Interscience, New York.

BLACKMAN, R. B., & TUKEY, J. W. 1958 *The Measurement of Power Spectra*. Dover, New York.

CAULFIELD, H. J., HAIMES, R. & CASASENT, D. 1980 Beyond matched filtering. *J. Optical Engng* **19**, 100–110.

DUNS, H. & ROS, N. C. J. 1963 Vertical flow of gas and liquid mixtures from boreholes. In *Sixth World Petroleum Congress*, Sect. 2, Paper 22. Frankfurt, West Germany.

GOVIER, G. W. & AZIZ, K. 1972 *The Flow of Complex Mixtures in Pipes*, p. 337. Van Nostrand Reinhold, New York.

GOVIER, G. W., RADFORD, B. A. & DUNN, J. S. C. 1957 The upwards vertical flow of air–water mixtures. *Can. J. Chem. Engng* 58–70.

GOVIER, G. W. & SHORT, W. L. 1958 The upward vertical flow of air–water mixtures. *Can. J. Chem. Engng* 195–202.

GRIFFITH, P. & WALLIS, G. B. 1961 Two-phase slug flow. *J. Heat Transfer* C 307–320.

HSU, Y. Y. *et al.* 1977 Proceedings of two-phase instrumentation. *Review Group Meeting*, NUREG-0375, January 1977.

HUBBARD, M. G. & DUKLER, A. E. 1966 The characterization of flow regimes for horizontal two-phase flow. *Proceedings of the* 1966 *Heat Transfer and Fluid Mechanics Institute, pp.* 100–121. *Stanford University Press.*

JONES, O. C. & ZUBER, N. 1975 The Interrelation between void fraction fluctuations and flow *patterns in two-phase flow. Int. J. Multiphase Flow*, **2**, 273–306.

KUTATELADZE, S. S., NAKORYAKOV, V. E., BURDUKOV, A. P., TATEVPSYAN, YU. V. & KUZ-MIN, V. A. 1972 Spectral characteristics of vertical two-phase flow. *Sov. Phys. Dokl.* **16**, 718–719.

LAHEY, R. T. Jr. 1978, A review of selected void fraction and phase velocity measurement techniques. In *Two-Phase Flow Measurements*, Fluid Dynamics Institute Short Course 78–1. Dartmouth College, Hanover, New Hampshire.

LAHEY, R. T. JR., MALAVIYA, B. K. & KRYCUK, G. 1978 A high intensity X-ray system for stochastic measurements of two-phase flows. *ANS Trans.* **30**, 497–499.

MALAVIYA, B. K. & LAHEY, R. T. JR., 1980 Analysis of the error in instantaneous void fraction measurements by a dual-beam X-ray technique. *ANS Trans.* **34**, 876–877.

NISHIKAWA, K., SEKOGUCHI, K. & FUKANO, T. 1969 On the pulsation phenomena in gas–liquid two-phase flow. *Bull. JSME* **12**, 1410–1416.

PIKE, R. W., WILKINS, B. & WARD, H. C. 1965 Measurement of the void fraction in two-phase flow by X-ray attenuation. *AIChE J.*, 794–800.

SMITH, A. V. 1971 Transient density measurements in two-phase flows using X-rays, *J. Br. Nucl. Engng Soc.* **10**, 99–106.

TAITEL, T., BORNEA, D. & DUKLER, A. E. 1980 Modeling flow pattern transitions for steady upward gas–liquid flow in vertical tubes. *AIChE J.* **26**, 345–354.

VINCE, M. A., & LAHEY, R. T. JR., 1980 Flow regime identification and void fraction measurement techniques in two-phase flow. NUREG/CR-1692, pp. 32–41.

YOUNG, T. Y. & CALVERT, T. W. 1974 *Classification, Estimation and Pattern Recognition.* Elsevier, Amsterdam.

ZUBER, N. & FINDLAY, J. A. 1965 Average volumetric concentration in two-phase flow systems. *J. Heat Transfer C* 453–468.